SANDIA REPORT
SAND2018-9708
Unlimited Release
Printed August 2018

Analysis of Cavern and Well Stability at the Bryan Mound SPR Site Using the M-D Salt Creep Model

Steven R. Sobolik

Prepared by
Sandia National Laboratories
Albuquerque, New Mexico 87185 and Livermore, California 94550

Sandia National Laboratories is a multimission laboratory managed and operated by National Technology and Engineering Solutions of Sandia, LLC., a wholly owned subsidiary of Honeywell International, Inc., for the U.S. Department of Energy's National Nuclear Security Administration under contract DE-NA0003525.

Issued by Sandia National Laboratories, operated for the United States Department of Energy by Sandia Corporation.

Available to DOE and DOE contractors from

U.S. Department of Energy
Office of Scientific and Technical Information
P.O. Box 62
Oak Ridge, TN 37831
Telephone: (865) 576-8401
Facsimile: (865) 576-5728
E-Mail: reports@osti.gov
Online ordering: http://www.osti.gov/scitech

Available to the public from

U.S. Department of Commerce
National Technical Information Service
5301 Shawnee Rd
Alexandria, VA 22312

Telephone: (800) 553-6847
Facsimile: (703) 605-6900
E-Mail: orders@ntis.gov
Online order: http://www.ntis.gov/search

SAND2018-9708
Unlimited Release
Printed August 2018

Analysis of Cavern and Well Stability at the Bryan Mound SPR Site Using the M-D Salt Creep Model

Steven R. Sobolik
Geotechnology and Engineering Center
Sandia National Laboratories
P.O. Box 5800
Albuquerque, New Mexico 87185-0751

ABSTRACT

This report presents computational analyses that simulate the structural response of caverns at the Strategic Petroleum Reserve Bryan Mound site. The cavern field comprises 20 caverns. Five caverns (1, 2, 4, and 5; 3 was later plugged and abandoned) were acquired from industry and have unusual shapes and a history dating back to 1946. The other 16 caverns (101-116) were leached according to SPR standards in the mid-1980s and have tall cylindrical shapes. The history of the caverns and their shapes are simulated in a 3-D geomechanics model of the site that predicts deformations, strains, and stresses. Historical wellhead pressures are used to calculate cavern pressures up through July 2016. Because of the extent of heterogeneous creep behavior observed throughout the Bryan Mound site, a set of cavern-specific creep coefficients was developed to produce better matches with measured cavern closure and surface subsidence. For this new implementation of the model, there are two significant advances: the use of the multimechanism deformation (M-D) salt creep model to evaluate both steady-state and transient salt creep; and the creation of finite element mesh geometries for the caverns that nearly exactly match the geometries obtained through sonar measurements. The results of the finite element model are interpreted to provide information on the current and future status of subsidence, well integrity, cavern stability, and drawdown availability.

The analyses shown in this report demonstrate that the use of sonar-based cavern geometries provide a more detailed evaluation of the effects of cavern pressure changes on stress behavior in the salt surrounding the cavern, and thus to evaluate long-term cavern integrity and evolution of drawdown availability. Some of the Bryan Mound caverns were shown to have less than five available drawdowns. Additionally, the choice of an alternate pressurization scenario for abandoned Cavern 3 gives further credence to the hypothesis that fluid is being forced up and out of the cavern into the caprock due to creep-induced closure. Finally, the model has been built with several options to allow for exploration of different parameter and operations scenarios; these will be particularly useful if a recent advance in the calculation speed using the M-D model is fully realized.

ACKNOWLEDGEMENTS

The authors would like to thank Anna Snider Lord, Byoung Yoon Park, Barry Roberts, Kirsten Chojnicki, and Dylan Moriarty, for their contributions to the work described in this report, and the U.S. Department of Energy, Strategic Petroleum Reserve office for their review and support of this work.

TABLE OF CONTENTS

LIST OF FIGURES

LIST OF TABLES

EXECUTIVE SUMMARY

This report presents he most recent computational analyses that simulate the structural response of caverns at the Strategic Petroleum Reserve Bryan Mound site. For this new implementation of the model, there are two significant advances. The first is the use of the multimechanism deformation (M-D) salt creep model to evaluate both steady-state and transient salt creep. This creep model represents the most current understanding of the mechanical behavior of salt in response to transients such as cavern pressure changes. The second is the creation of finite element mesh geometries for the caverns that nearly exactly match the geometries obtained through sonar measurements. The mesh construction for the caverns implements a new patent-pending process that creates a mesh geometry that matches nearly exactly the cavern geometry measured via sonars (Park et al., 2017 & 2018). This feature is particularly important for caverns with unusual geometric features, such as significant protuberances in Caverns 103 and 105, and the lower and upper lobes on Cavern 5. Another feature that has been built into the model, and will be utilized in future analyses, is the construction of separate regions of caprock which are undamaged or damaged by steam-injection sulfur mining in the early 20th century. Other continuing features include the use of historical wellhead pressures to determine cavern pressures, cavern-specific creep properties, separate regions of hard and soft salt on either side of a prominent boundary shear zone, and the inclusion of five full-drawdown leach layers for near all the caverns.

The results of the computational analyses lead to the following conclusions regarding the model itself, and the conditions of the caverns at Bryan Mound:

- The addition of realistic cavern geometries to the computational mesh has contributed to identification of specific cavern regions, such as in Caverns 103 and 105, which will experience long-term dilatant and tensile stress conditions due to their geometries.
- As a result, the baseline number of available drawdowns for several caverns has been reduced from five to a lower number, based on the evolution of dilatant and tensile stresses around certain caverns through planned workover and drawdown activities (Sobolik et al., 2018).
- Surface subsidence measurements continue to indicate that some phenomenon is occurring to cause enhanced subsidence over Cavern 3. A hypothesis based on previous analyses assumes that the reason for this is that brine is being forced upward from the cavern into the caprock due to creep-induced pressurization in the cavern. This behavior would correspond to a brine head in the borehole extending only up to the caprock/salt interface or slightly higher. In these calculations, a brine head for Cavern 3 was simulated to extend to above the caprock; the resulting predictions did not show a subsidence maximum over Cavern 3. These results lend credence to the hypothesis that the brine from Cavern 3 is able to enter the caprock just above the salt interface.
- The set of salt creep model properties for the new model results in predicted cavern volume reduction behavior that matches CAVEMAN-derived closure data much better than the previous Bryan Mound models. However, the resulting predictions for surface subsidence are significantly larger than the periodic subsidence data indicate.

The new model represents a more realistic assessment of the behavior of the Bryan Mound site. However, uncertainty still exists regarding several aspects of the model, and how they pertain to operational issues at the site. The types of uncertainty include the following items which will be addressed in future work:

- The algorithm used in CAVEMAN to calculate the daily changes to cavern volumes based on wellhead pressures, fluid temperatures, the depth of the oil/brine interface, and the geometry of the cavern, is scientifically sound. However, the parameters used in that algorithm have never been satisfactorily validated in comparison with known quantities of fluid movements into and out of the cavern. Before a new effort to develop a site-wide, cavern-specific set of salt creep parameters begins, it will be necessary to complete a study of CAVEMAN in comparison with site data to validate the algorithm and its parameters. Once there is a new historical timeline of cavern volume closure in which more confidence can be given, then a new property set in the geomechanical model may be developed, which will hopefully provide better agreement with both cavern closure and surface subsidence.
- The new model takes significantly more CPU time to run than the 2009-2012 model. This is due to a combination of factors – approximately 50% more elements in the mesh, the high aspect ratio of many elements due to the unusual cavern geometry to which they were mapped, the use of historical pressure fluctuations rather than relatively constant cavern pressures, and the use of the M-D creep model to capture transient effects. The last item regarding the M-D model may be improved soon, as members of the Sandia computational sciences department have developed a new algorithm for calculating the strain rates in the M-D model that have reduced computation time by 90%, while producing essentially the same results. The calculations in this report will be re-run with the new version of the model; if the results are the same and the computing performance is improved to the promised scale, then the model will have much greater utility for use in property parameterization.
- A model with improved runtime will be useful for evaluating different concepts of the effects of damage to the caprock. The model includes section of caprock that are identified as having been damaged due to sulfur mining. Previous analyses (Sobolik, 2010; Sobolik & Ehgartner, 2012b) indicated that stresses in undamaged sections of caprock may be higher than in damaged sections, as the undamaged areas much take up more of the overburden load. This could result in mechanical damage to borehole casings in those areas. Several Bryan Mound wellbores have experienced damage in the caprock, and this model should be exercised to determine if it can predict damage in those and other locations.
- A model with improved runtime performance will also be useful for scenario analysis of Cavern 3 behavior.

1. INTRODUCTION

1.1 OBJECTIVE

The U.S. Department of Energy (DOE) Strategic Petroleum Reserve (SPR) stores crude oil in solution-mined caverns in the salt dome formations of the Gulf Coast. There is a total of 60 caverns located at four different sites in Texas (Bryan Mound and Big Hill) and Louisiana (Bayou Choctaw and West Hackberry), as shown in Figure 1. Each cavern is constructed by drilling one or more boreholes into the salt dome and injecting fresh water. The fresh water dissolves the salt and creates brine, which is then pumped out of the cavern. This process, which is known as leaching, creates a brine-filled volume in the salt that is eventually used for the storage of oil. The boreholes (or wells) of the cavern are then lined with steel casings cemented in place from the surface to near the top of the cavern. The safe and effective operation of the storage caverns requires technical issues to be addressed in order to maintain the integrity of the caverns and their wells. The Bryan Mound salt dome, located approximately 60 miles south of Houston, Texas, near the city of Freeport, is the largest of the SPR sites in terms of oil-storage capacity (currently 226 million barrels). Sandia National Laboratories (SNL), as the geotechnical advisor to the DOE SPR Project Office, conducts site-characterization investigations and other longer-term geotechnical and engineering studies in support of the program.

The SPR sites, as well as most other oil and natural gas storage sites in salt domes along the Gulf Coast, are varied in terms of cavern structure and layout. The Bryan Mound SPR site was acquired by DOE, by condemnation, in April 1977 from the Freeport Mineral Company and other owners. At that time there were five caverns at the site. An analysis of these existing Phase 1 caverns from 1977 to 1979 resulted in four of them, Caverns 1, 2, 4, and 5, being certified for crude oil storage. As early as October 1977 oil injection commenced at the site. After purchase of the site, additional caverns were leached using standards that resulted in tall cylindrical shaped caverns; these caverns, numbered 101 through 116, are referred to in this report as Phase 2 or post-1981 caverns. The Bryan Mound salt dome includes at least three boundary shear zones, which tend to divide the dome into zones of high and low salt creep potential. However, creep rates as measured by cavern closures vary significantly throughout the salt dome. Furthermore, sulfur mining in the caprock at Bryan Mound occurred in the early 20th century (Kirby & Lord, 2015). Sulfur mining was performed using the Frasch extraction method, for which superheated steam at 320°F was injected into the caprock to draw out sulfur, in a mostly molten form with some SO_2 and H_2SO_4. This mining method both weakens the in situ rock and removes material, and thus induces underground collapse and subsidence; in the case of Bryan Mound, evidence of this subsidence is indirect, with no known monitoring program. The one Phase 1 cavern not selected for oil storage, Cavern 3, was filled with brine, plugged and abandoned in 1980. The effect of its presence on surface subsidence and salt dome structural integrity has been analyzed in previous Sandia analyses of the Bryan Mound site (Sobolik & Ehgartner, 2009, 2012a & 2012b; Sobolik and Lord, 2014). Cavern 2 at Bryan Mound was decommissioned in 2016, with the oil removed and replaced with brine. The cavern is pressurized at normal operating pressure to maintain cavern integrity.

Figure 1. Locations of SPR sites.

SNL has performed several previous analyses that model the behavior of the caverns in the Bryan Mound salt dome, and evaluate possible effects on site operations such as potential casing failures. The first analysis (Sobolik and Ehgartner, 2009) described three-dimensional (3-D) geomechanical calculations modeling the long-term behavior of the Bryan Mound SPR site in response to changing oil pressure conditions in the storage caverns and future growth of the caverns through subsequent leaching. The 2009 analysis also evaluated the stress and deformation history of the caverns to the present day, and predicted the effects on cavern stability and well strain of subsequently enlarging the caverns. Those calculations used a computational mesh that included a geometrically-realistic rendition of the Bryan Mound salt dome, and sonar-based, axisymmetric representations of the vast majority of the oil storage caverns. Sobolik and Ehgartner (2009) also assumed a homogeneous, elastic caprock layer, and a linear temperature distribution as a function of depth based on measurements from deep in the salt dome. Long-term cavern performance was evaluated using four performance measures: a dilatant damage criterion based on deviatoric stress; cavern volume closure; axial well strain in the caprock; and maximum surface subsidence above each cavern. Because of the large variability of salt creep properties throughout the Bryan Mound salt dome, there was a similarly large variability in the correlation between measured and predicted cavern closure and surface subsidence rates.

Sobolik and Ehgartner (2009) predicted elongation along the boreholes casings and liners that resulted in axial strains in the caprock section not exceeding the prescribed threshold strains of 0.2 millistrains for cement and 1.6 millistrains for steel casings. They also predict axial strains in the salt that exceed the cement liner threshold value, but not the steel casing threshold. These

analytical results came into question when several well casings at the Bryan Mound site experienced failures of various types. None of the documented failures appeared to be a joint separation due to excessive elongation, which would have been the type most expected. Instead, the failures appeared to be one of several varieties: outward bowing of the walls of the casing due to axial compression; intrusion of cement or steel into the wellbore; or shear failure due to horizontal shear or twisting stresses. These failures made it obvious that the caprock in which these casings are installed is not behaving as previously modeled, and that unusual stresses are being generated at the casings. Therefore, a new analysis was conducted (Sobolik, 2010) for which a series of sensitivity studies was performed, altering the mechanical properties of selected sections of the caprock. These calculations were performed using a 30-degree wedge to simulate a symmetric 19-cavern field geometry, with the caprock divided into concentric sections to easily allow for some spatial variability of caprock mechanical properties. Sobolik (2010) identified regions of higher probability of casing damage in the caprock due to proximity to sulfur mining wells and temperature in the caprock, and created a prioritization list for inspection of wells based on several factors.

The observation that the subsidence over Cavern 3 is greater than over the rest of the Bryan Mound site has been documented for several years (Osnes, 1995; Bauer, 1999; Lord, 2007a). Recently, erratic surface subsidence measurements in the vicinity of Cavern 3 have been observed (Lord, 2009 and 2010). Recent evaluation of the surface subsidence data indicates that the measurements taken at Bryan Mound in January 2007 may have been inaccurate over the entire site. If the data from that month are ignored, the subsidence rate over between 2005 and 2010 looks much closer to the rates previously observed. Nevertheless, while there have been no signs of damage resulting from a possible increase in subsidence activity over Cavern 3, longstanding concerns of the effects of the cavern on the stability of surrounding caverns were increased. A new set of calculations was performed to include Cavern 3 in the computational model for Bryan Mound (Sobolik and Ehgartner, 2012). The purpose of the analysis was to evaluate the stability of Cavern 3, its potential effect on nearby wellbores and surface facilities, and the zone of impact on surface if Cavern 3 were to fail. The entire lives of the caverns (construction, brine or oil storage, operating and workover pressures) were modeled individually for each cavern. The temperature distribution was modified to more closely match measured temperatures in the salt close to the caprock, which are higher than normal due to residual heat remaining from the sulfur mining activities.

The conceptual and computational model for this new set of calculations includes several changes that allow greater accuracy in the geometric representation of the caverns, an upgrade to the multi-deformation salt creep model, and several options for modeling different sections of the caprock with varying physical properties to account for the effects of sulfur mining and its resulting void formation.

1.2 REPORT ORGANIZATION

This report is organized in the following fashion: Section 2 gives a brief description of the Bryan Mound cavern site to show the diversity of cavern geometries. Section 3 describes the analytical model, including the cavern designs, stratigraphy, material models and properties, and damage

criteria used for the analyses. Section 4 shows the results of the calculations, including forecasting future mechanical behavior, identifies failure modes for the salt and the casings, and briefly discusses the updated assessment of available drawdowns for each cavern. Section 5 summarizes the results, and provides concluding remarks.

2. SITE DESCRIPTION

The Bryan Mound salt dome, located approximately 60 miles south of Houston, Texas, near the city of Freeport, is the largest of the SPR sites in terms of oil-storage capacity (currently 226 million barrels). The geological characteristics related to the Bryan Mound site were first described by Hogan (1980). Neal et al. (1994) utilized the earlier work, together with additional information on dome geology, surrounding stratigraphy, and relevant environmental information, to update the dome characterization. Conversion of the two-dimensional databases from these earlier characterization reports formed the basis for the most recent reexamination by Stein and Rautman (2005) using modern three-dimensional methods for representation of the dome and its surroundings. While major aspects of the dome, caprock and surrounding strata defined by the earlier characterizations remain unchanged, the updated three-dimensional models of Stein and Rautman (2005) used more refined analysis of the data and produced models of the dome that differed slightly from the earlier models. The three-dimensional models also achieve a level of visualization clarity and graphical manipulation previously impossible. Finally, the Bryan Mound caverns have been extensively characterized and mapped in a sonar atlas prepared by Lord (2007b).

Figure 2 shows a plan view of the Bryan Mound site (Stein and Rautman, 2005) with the caverns' approximate location within the salt dome, and the interface of the salt dome with the caprock and surrounding sandstone. The approximate cavern locations are shown in the plan view. An updated geologic perspective of the salt dome and caprock are provided in Figure 3 (Lord, 2007b). Note that there seem to be two regions within the salt dome that are possibly separated by a salt spine or shear zone. The thickest caprock regions correspond to the two separate regions inferred from the structure contour map. Further study of the sonar data used to characterize the salt dome reveal the orientation of potential boundary shear zones within the salt dome; these zones are shown in Figure 4 (Lord, 2007b). Of the three boundary shear zones shown in Figure 4, the one of greatest interest is that which is in the southeast portion of the salt dome, running roughly southwest to northeast. Caverns 106, 109, 112, 113, and 114 are located to the south of this shear zone. This region of the salt dome appears to contain salt with creep properties leading to higher creep rates than the remainder of the dome; Sobolik and Ehgartner (2009) took this into account and created a computational mesh with a salt dome along this shear zone. Cavern 3 can be seen in Figure 4 as the largest cavern at the western edge of the dome.

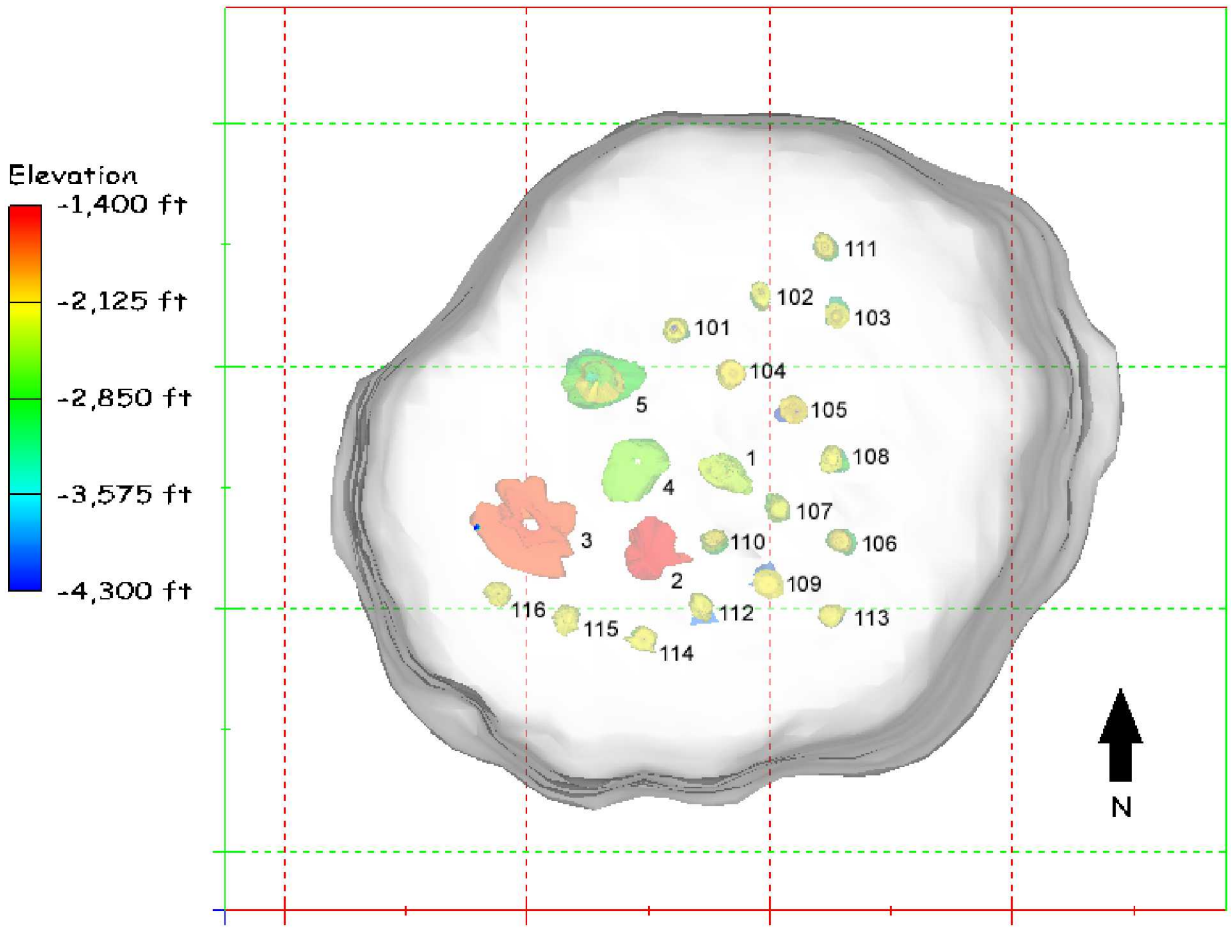

Figure 2. Top view of the Bryan Mound salt dome and selected cavern models. (Lord, 2007b)

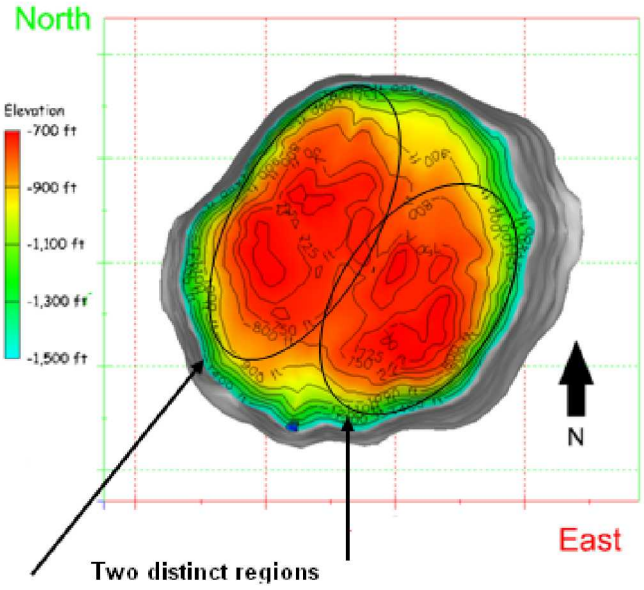

Figure 3. 3-D model of the top of caprock and the top of salt (considered to be the bottom of caprock); contours are of caprock elevation in feet (Lord, 2007b).

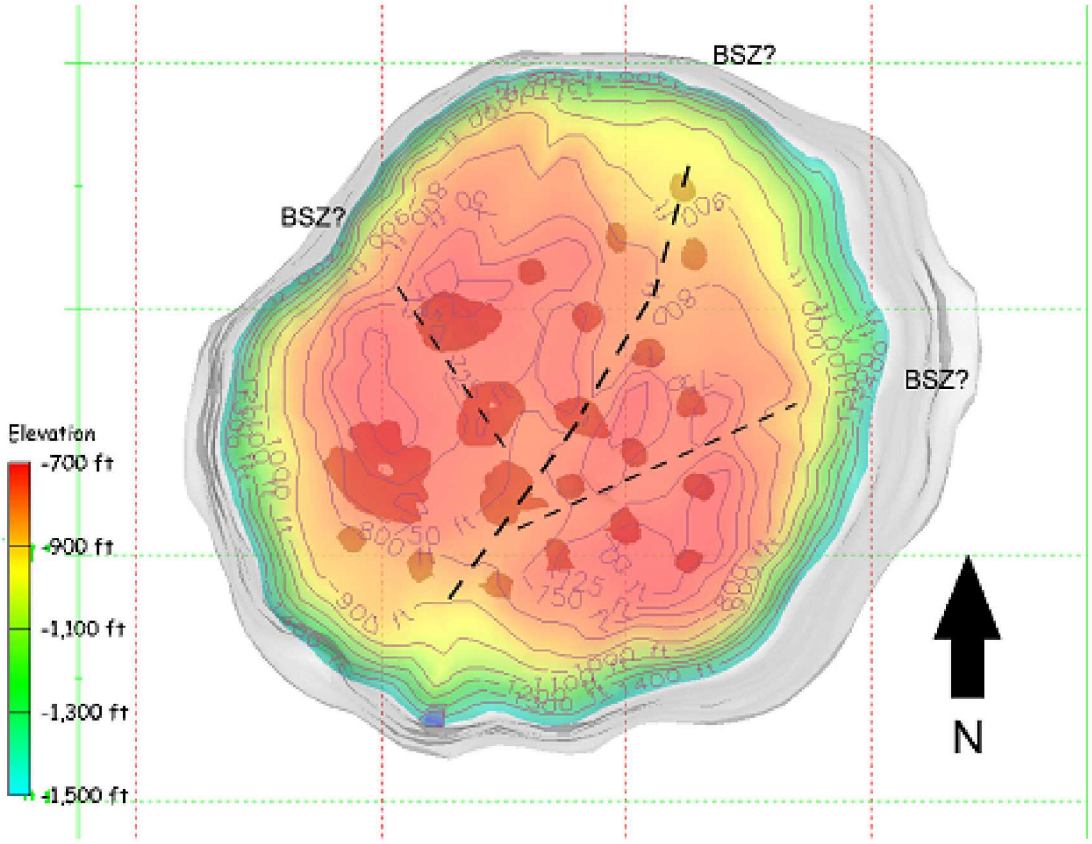

Figure 4. Potential boundary shear zones in the Bryan Mound salt dome (Lord, 2007b).

Figure 5 shows the cavern layout at the Bryan Mound site (Rautman and Lord, 2007), using the DOE coordinates provided; Cavern 4 is located in the cluster of cavern wells between caverns 1, 2, 3, and 5. Figure 6 shows oil storage cavern geometries based on sonar measurements obtained through 2007 (Rautman and Lord, 2007). Note the enlarged tops and asymmetries of the cavern shapes. In general, caverns in the SPR are intentionally shaped with larger tops to accommodate future oil drawdowns where only the bottom portions of the caverns are preferentially leached, and hence the overall cavern shape becomes more cylindrical, due to raw water injections to remove the oil. Salt properties also result in unpredictable cavern shapes as the insoluble content (primarily anhydrite) or dissolution rates of salt can spatially vary. This explains some of the asymmetries found in the cavern shapes. The Phase 1 caverns were acquired through purchase; these caverns have unusual shapes as they were not intentionally leached for product storage, but were used to produce brine.

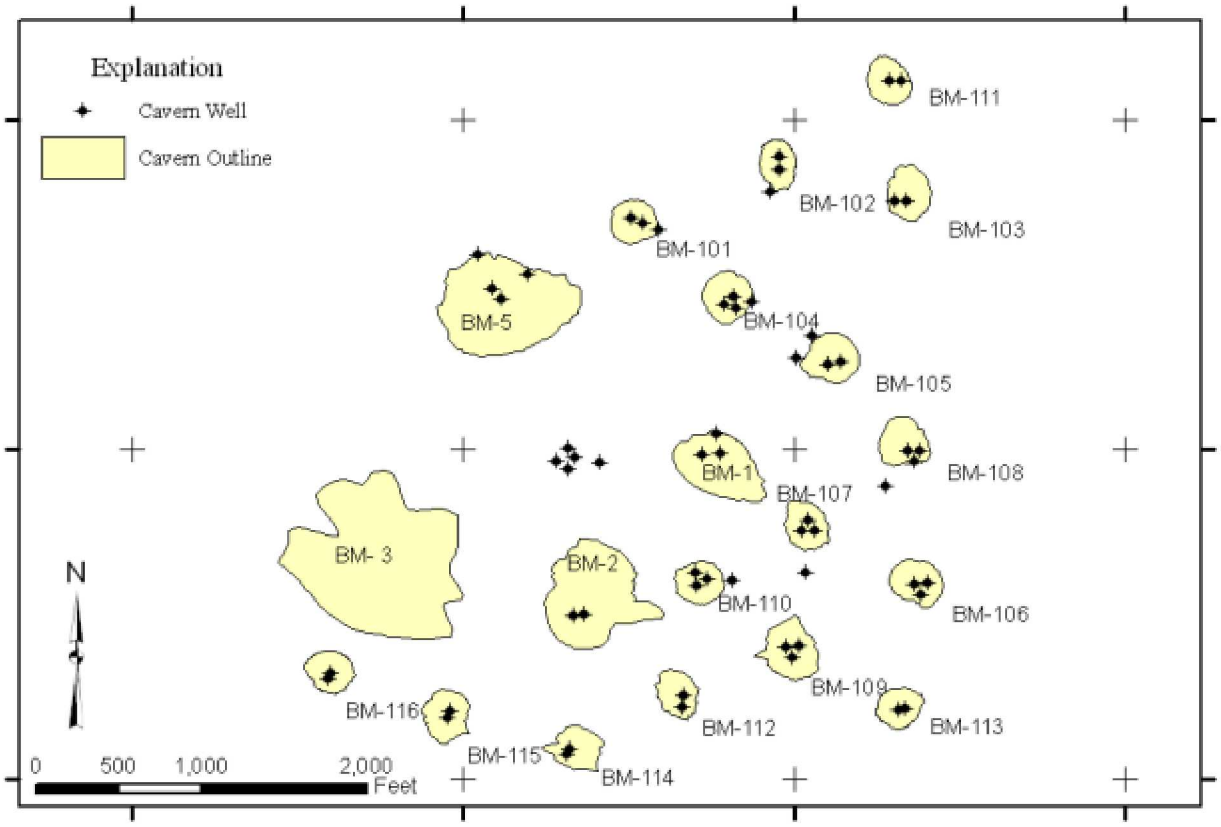

Figure 5. Schematic of the Location of the SPR Caverns at Bryan Mound (Rautman and Lord, 2007)

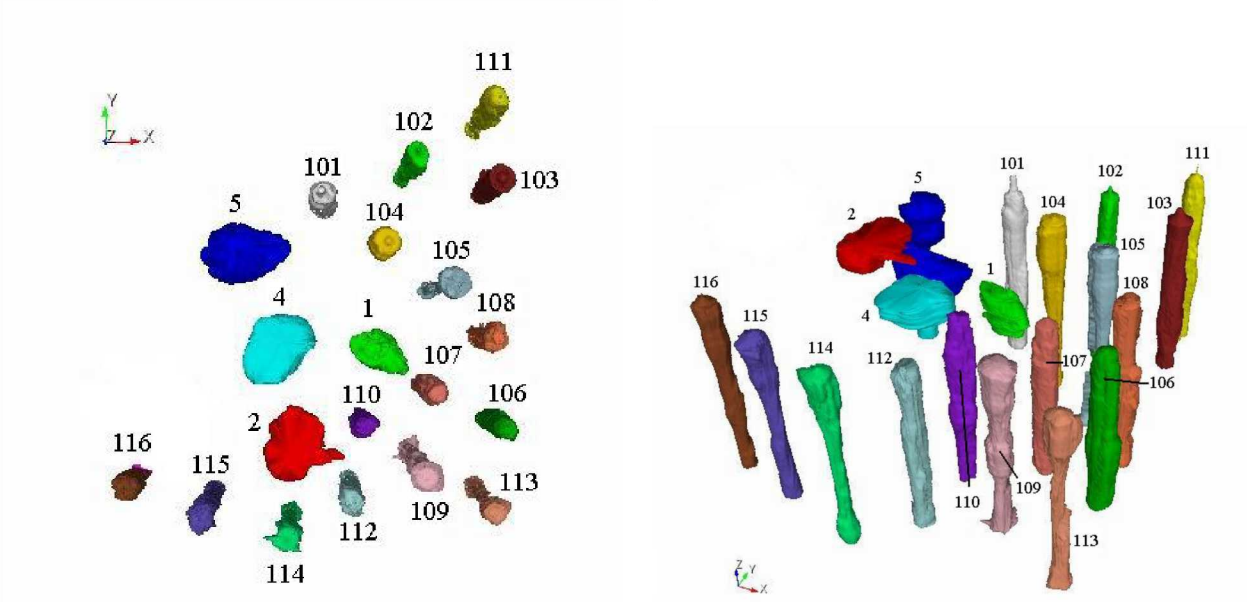

Figure 6. Visualization of the 20 oil-storage caverns at Bryan Mound SPR site.

The Bryan Mound caprock was subjected to extensive sulfur mining prior to the development of the Strategic Petroleum Reserve. The caprock was mined in the 1910s-1920s using the Frasch technique, for which steam was injected into the caprock to leach out the sulfur to be pumped out

to the surface. The long-term consequences of the sulfur mining include a large latent temperature perturbation in the caprock and upper 40-60 feet of the salt dome, the presence of sulfuric acid in the caprock, and significant volumes of void space from the removal of sulfur. These voids are the most likely explanation for lost circulation encountered in boreholes drilled into the salt dome during cavern formation. Figure 7 is an overlay map indicating the regions where most of the sulfur mining boreholes were drilled, and identifying the SPR caverns where lost circulation was encountered during drilling (Kirby and Lord, 2015).

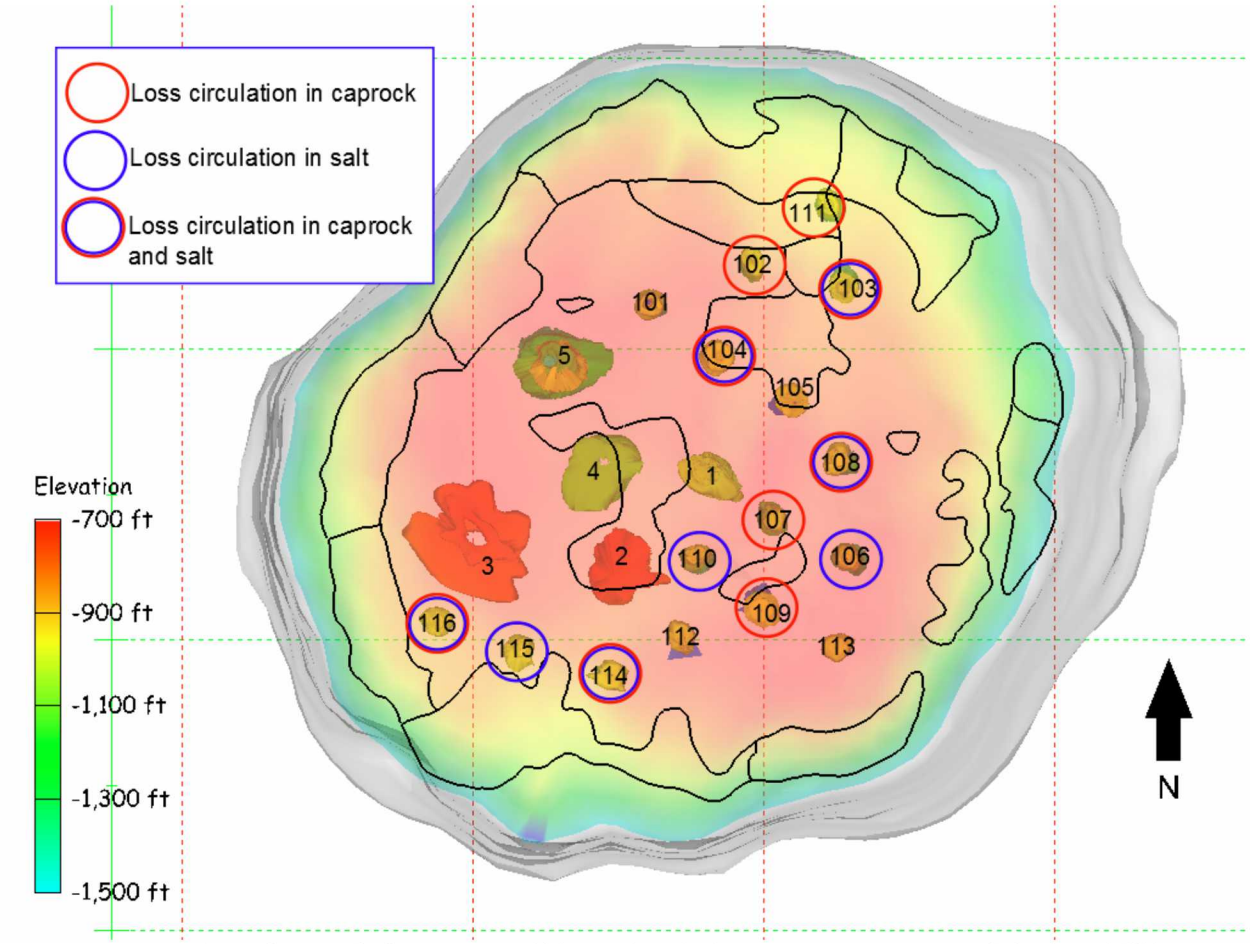

Figure 7. Plot of recorded cavern well loss circulation zones encountered during drilling.

Cavern 3, located in the southwestern quadrant of the dome (Figures 4 and 5), was initially developed by Dow in 1942 as one of five caverns in the Bryan Mound salt dome for brine production in the period 1942 to 1957. Four of these caverns (Caverns 1, 2, 4 and 5) were purchased by the DOE in 1977 and certified as suitable for oil storage by Gulf Interstate Engineering Company (GIEC). Cavern 3 was shut down in 1957 due to its large roof span. Cavern 3 contains a volume of 6.4 MMB based upon a 1979 sonar survey. The roof is highly irregular and the maximum diameter of the cavern (~1350') is the largest of any of the DOE owned caverns. About two years after it was shut down, the pressure dropped. Testing by Dow showed the well had hydraulic integrity, but not the cavern. The original 8-3/8" production casing failed in the mid-1950s, and a 5-1/2" in casing was cemented in. Dow believed the cavern was in communication with the top of salt. GIEC performed a number of tests (fluid level

and brine sampling) and ran various cased hole logs in Cavern 3 in 1977. The cavern was not certified and the test results were not formally reported as were the results from the other caverns which were certified (Keplinger and Associates, 1980; Hogan, 1980). Brine samples taken at three different times between November 1977 and April 1978 showed significant variations in composition suggesting that circulation was occurring in the cavern. Later tests performed by Keplinger for SPR to determine fresh water circulation within the cavern were inconclusive, but the fact remained that the cavern did not hold pressure and therefore was not recommended for oil storage (Keplinger and Associates, 1980). Hogan (1980) and Preece and Foley (1984) performed computational analyses of Cavern 3. Both studies concluded that Cavern 3 was structurally stable, and neither study predicted tensile stresses in the roof of the cavern. Neither study indicated that Cavern 3 was hydraulically stable, and both studies agreed with the recommendation that Cavern 3 should not be used for oil storage. Additionally, three surveys of the wells at Cavern 3 noted the presence of a void in the caprock of several feet in height at around 818 feet depth, and the height of the void decreased in succeeding reports (Keplinger and Associates, 1980 included the latest of these surveys). This void in the caprock has been assumed to have resulted from the sulfur mining at Bryan Mound.

3. ANALYSIS MODEL

3.1 MODEL DESCRIPTION

This analysis uses much of the same mesh generation and simulation methodologies as were used for previous analyses of Bryan Mound (Sobolik & Ehgartner, 2009, 2012a & 2012b; Sobolik and Lord, 2014). The new model includes many new enhancements involving the following elements:

- Mesh construction for the caverns implements a new patent-pending process that creates a mesh geometry that matches nearly exactly the cavern geometry measured via sonars (Park et al., 2017 & 2018). This is described in Section 3.2.
- Mesh construction for the caprock creates zones in the caprock that match the mapped areas of sulfur mining illustrated in Figure 7. This construction allows for the option of performing multiple simulations in which the material properties of the mined areas may be modified to evaluate the effects of borehole casings throughout the site. This mesh development is described further in Section 3.2.
- An improved implementation of the M-D model in Sierra/Adagio, which is described in Section 3.3.
- The use of historical cavern pressures in the simulation, so that predicted cavern closure and surface subsidence results may be more directly compared to site data. This comparison was used to develop a set of cavern-specific creep properties for this analysis; this process and those properties are described in Section 3.4.
- Previous analyses evaluated the cause of increased subsidence over abandoned Cavern 3 by simulating different cavern pressure behaviors in the cavern correlating to a hypothesized leak of fluid up the borehole to the caprock. This capability was maintained in the new model, but for the analyses presented in this report the cavern pressure was maintained at a constant low value.
- Material properties used for the non-salt materials are described in Section 3.5, and the use of a dilatant stress damage factor (safety factor) is described in Section 3.6.

The history of the caverns is an important component of the model. At the Bryan Mound site, the five caverns known as Phase 1 – Caverns 1 through 5 – were created as early as 1946 and were used for brining and storage before the SPR took ownership of them in 1981. Cavern 3 was eventually filled with brine, plugged and abandoned. The analysis simulates the leaching of these caverns to full size over one year each, then filled with brine until 1981 and afterward filled with oil. Beginning in 1981, sixteen other storage caverns were created over a seven-year period. The analysis also simulates the leaching of the post-1981 caverns and subsequent filling with oil. In general, these caverns are maintained at constant operating pressure ranges except during workovers. The default pressure condition applied to each cavern is based on an average wellhead pressure ranging between 900 and 975 psi. For the simulation of cavern pressures during the life of the site, three stages are defined: the years prior to 1990, for which no wellhead pressure data were saved and so an estimate is made; the period between 1/1/1990 and 7/26/2016, for which historical data are used; and the future beyond 2016, for which the same algorithm from the first stage is used. For the first pressure stage beginning in the simulation year 1984, a series of five-year cycles of cavern workovers was initiated. During the five-year

cycle, every cavern is scheduled for a workover. During the workover, the affected cavern is held at 0 psi wellhead pressure for three months. The pressures for all caverns are at normal operating pressure for the fourth month (so that the workover rig can be moved to a new well) and then the workover of the next scheduled well begins. Previous analyses have shown that the abrupt pressure drop during the workover are the times for greatest potential for damage to the cavern wall and borehole casings. The duration of the simulated workover may be slightly longer than is typically encountered in the field, but is chosen to provide an adverse condition and closely simulate actual subsidence measurements, which reflect periods of low to intermediate operating pressures associated with fluid transfers. During the historical pressure period, workovers are reflected in the data during the times that the wellhead pressure is near zero.

3.2 STRATIGRAPHY AND COMPUTATIONAL MESH

The mesh developed for the computational model is illustrated in Figures 8 and 9. This mesh simulates the entire salt dome geometry. Figure 8 shows the entire mesh used for these calculations, and Figure 9 shows the same view with the overburden and surrounding rock removed to expose the caprock and salt formations. This mesh contained 7.9 million elements. Six material blocks are used in the model to describe the stratigraphic layers: the overburden, unmined and mined sections of the caprock, two sections of the salt dome designated “hard” and “soft” salt based on observed creep deformation rates, and the rock layers surrounding the salt dome. Sobolik and Ehgartner (2009) determined that the Bryan Mound salt dome would be best modeled by dividing it into “hard” and “soft” sections, based on the observed cavern volume closures at the site and on the existence of the shear zone boundary shown in Figure 4. The overburden is made of sand, and the caprock layer is made of gypsum or limestone. The overburden and caprock thicknesses are reasonably constant over the entire salt dome, so for meshing purposes they have been given constant values (Neal et al., 1994; Lord, 2007b); the overburden layer is 760 feet thick, and the caprock 280 feet thick. However, certain sections of caprock comprising the bottom 100 feet of the layer and matching the lost circulation zones in Figure 7 were created as a separate material block so that the effects of weakened caprock in that section may be evaluated. Figure 10 shows different views of the caprock section to show how they were incorpoarted into the mesh. The rock layers surrounding the salt dome comprised several layers of sandstone and shale; they have been modeled as one large layer of sandstone due to the minimal deviation in densities and rock mass moduli throughout those layers. The post-1981 caverns were typically constructed on 750-feet center-to-center spacings. Table 1 lists the cavern coordinates, top-of-cavern depths, and initial heights and volumes used in the analysis. The coordinates are based on Texas field coordinates, and converted to mesh coordinates with Cavern 1 at the origin, and coordinate axes aligned with compass directions (X-axis for W-E, Y-axis for N-S).

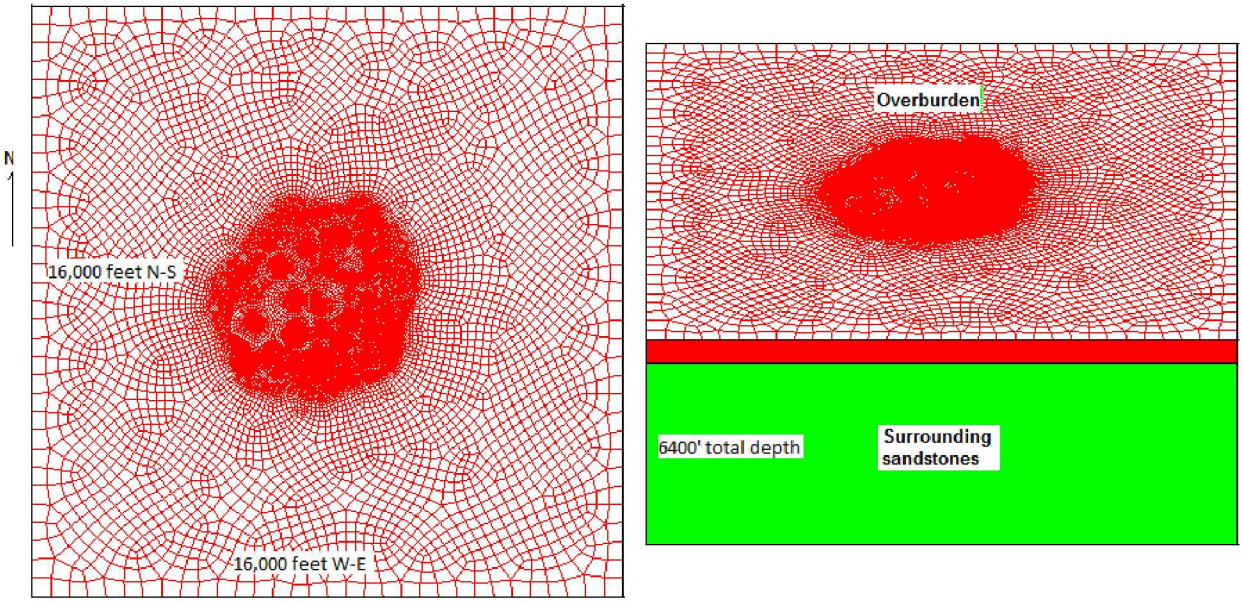

Figure 8. Computational mesh developed for the Bryan Mound calculations.

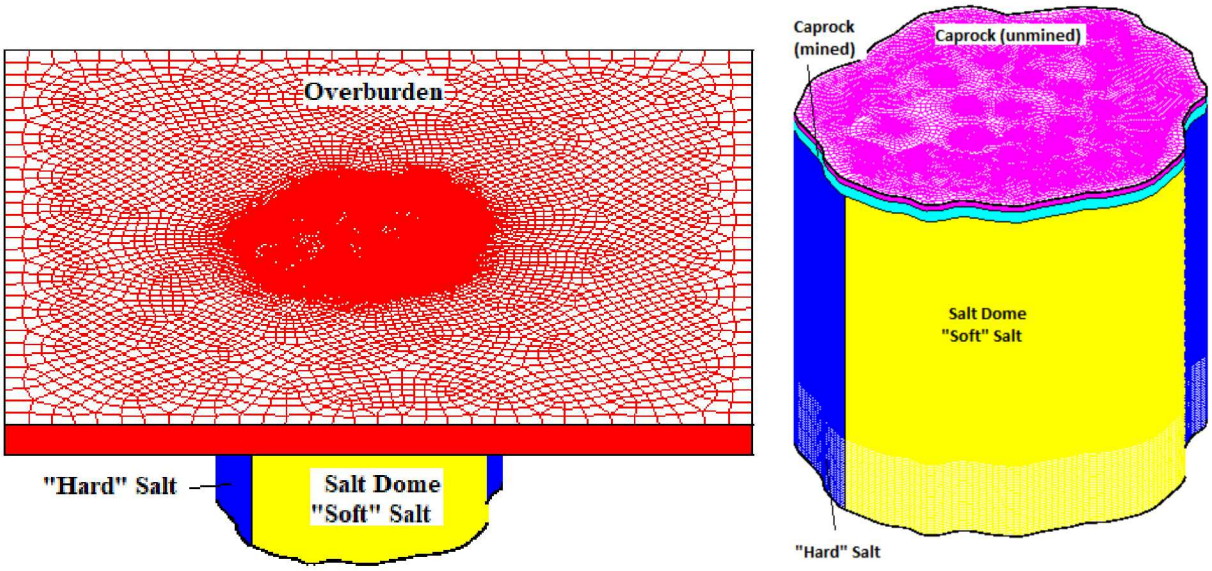

Figure 9. Computational mesh showing the salt formation and caprock.

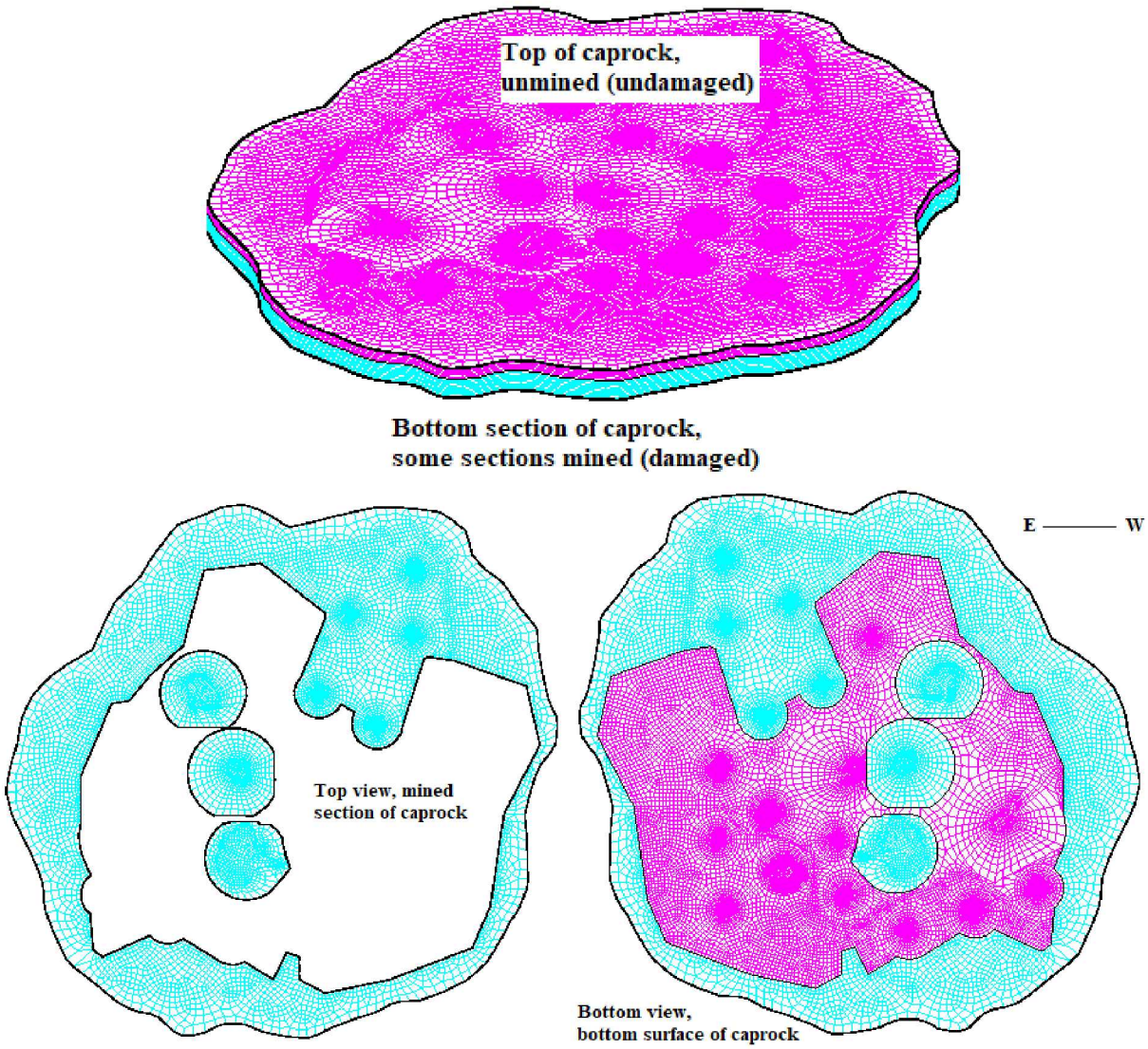

Figure 10. Top and bottom views of the computational mesh for the unmined/undamaged caprock (magenta) and mined/damaged caprock (cyan).

Table 1. Cavern coordinates, depths, heights, and construction dates used in the model.

Bryan Mound Cavern	X, feet (positive X is West)	Y, feet (pos. Y is North)	Depth to Ceiling, feet	Initial Height, feet	Initial Volume, MMB (1993)	Begin Construct (approx)	End Construct (approx)	Begin Oil Storage (approx)
1	0	0	2349	413	8.46	1/1/1946	1/1/1947	10/1/1978
2	-829.881	-988.094	1450	220	6.32	1/1/1946	1/1/1947	2/1/1978
4	-904.481	23.80583	2495	581	20.68	1/1/1946	1/1/1947	1/1/1978
5	-1334.58	924.5058	2102	1171	37.87	1/1/1957	1/1/1958	1/1/1984
101	-546.781	1415.506	1998	2161	11.23	9/1/1982	9/1/1984	9/1/1984
102	347.2786	1785.598	2203	2034	11.52	1/1/1981	5/1/1984	5/1/1984
103	1116.697	1518.731	2122	2011	11.43	5/1/1982	5/1/1984	5/1/1984
104	70.43307	942.4114	2108	2055	11.7	1/1/1981	1/1/1983	1/1/1983
105	716.3358	544.0781	2050	2143	11.39	1/1/1981	7/25/1983	7/25/1983
106	1165.614	-800.839	2106	1905	12.45	1/1/1981	1/1/1983	1/1/1983
107	518.3775	-412.311	2150	1947	11.4	1/1/1981	1/1/1983	1/1/1983
108	1121.391	5.522499	2166	1964	12.17	9/1/1983	9/1/1985	9/1/1985
109	426.9886	-1245.69	2132	2044	11.57	7/1/1981	7/25/1983	7/25/1983
110	-153.281	-807.794	2140	1982	11.42	1/1/1981	1/1/1983	1/1/1983
111	1095.296	2266.909	2130	1998	11.21	1/1/1983	3/1/1984	3/1/1984
112	-241.881	-1550.89	2065	2040	10.98	12/2/1982	11/30/1984	11/30/1984
113	1066.019	-1562.79	2134	2066	7.07	1/1/1984	10/31/1985	10/31/1985
114	-856.484	-1799.09	2130	2036	8.23	8/1/1985	8/1/1987	8/1/1987
115	-1642.52	-1571.86	2146	1984	10.32	9/1/1984	8/1/1986	8/1/1986
116	-2359.92	-1338.53	2100	1845	10.74	8/1/1984	8/1/1986	8/1/1986
3	-2008.08	-701.695	1560	120	6.44	1/1/1946	1/1/1947	P&A

Figure 11 shows three views of the layout of the meshed caverns used for these calculations: a view showing their placement within the salt dome, and views showing the geometry of the caverns. These figures represent a significant enhancement to the meshing capability for Sandia's geomechanical analyses. The construction of the finite element mesh for the caverns implements a new process that creates a mesh geometry that matches nearly exactly the cavern geometry measured via sonars (Park et al., 2017 & 2018). The Sandia mesh generation program CUBIT is used to create the mesh (Blacker et al., 2016). This process utilizes the fact that sonar data are usually taken at intervals of 20 feet as the instrument goes downward in the cavern. The geometry of these 20-foot sections forms the boundaries of the cavern mesh for the corresponding 20-foot sections. A mesh is generated for that section, and the nodal geometry for the individual elements is smoothed to produce the highest-quality hexahedral (6 sides, 8 nodes) elements possible using algorithms within CUBIT. The nodal geometry generated on the bottom of one 20-foot section is used for the nodal geometry on the top of the underlying section, thus maintaining nodal integrity throughout the mesh. This capability also allows the generation of several pre-defined leach layers, or "onion-skin" layers, that represent the salt removed from a cavern during a drawdown process (when the oil in a cavern is removed with fresh water, which dissolves or leaches salt from the cavern wall). A typical rule-of-thumb (based on historical operations) is that the amount of salt removed from a cavern during a drawdown is about 15% of the volume of fresh water pumped into the cavern. Thus, the onion skins built into the mesh typically represent 15% progressive increases in the cavern volume along the entire height of the

cavern. For this analysis, five leach layers have been constructed for each cavern except for caverns 2, 3, and 5 for operational reasons. Finally, the caverns and their leach layers have been constructed within a cylinder that fits into the holes in the mesh shown in the top part of Figure 11. These cylinders allow for block-specific designation of creep parameters for the purpose of trying to match historical cavern volume loss based on cavern pressure histories. Figures 12 and 13 highlight two caverns, 103 and 105, and show the full cavern from four direction and cutaway views of the cavern, onion skin, and cylinder meshes.

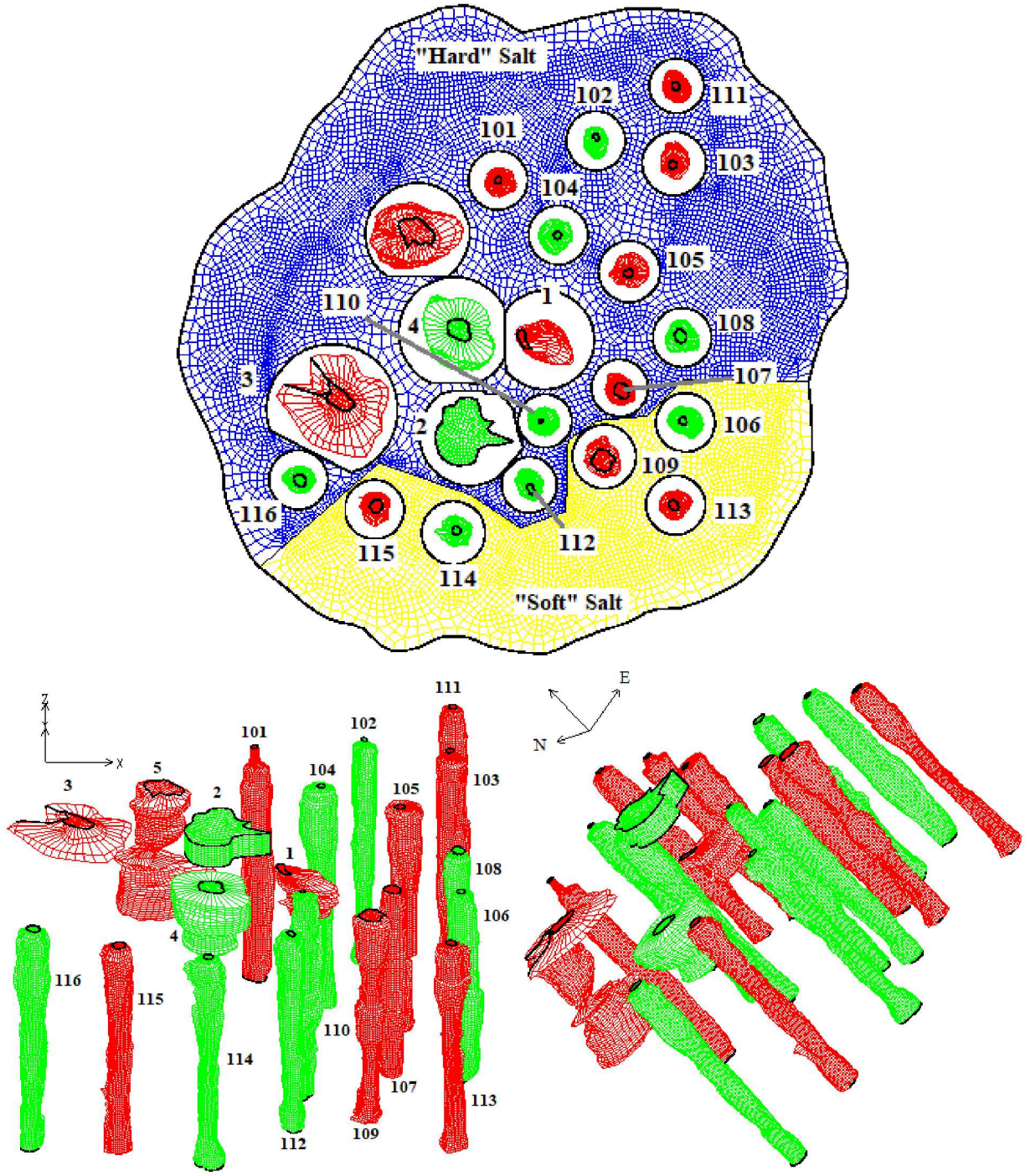

Figure 11. Bryan Mound caverns included in the computational mesh (3 views).

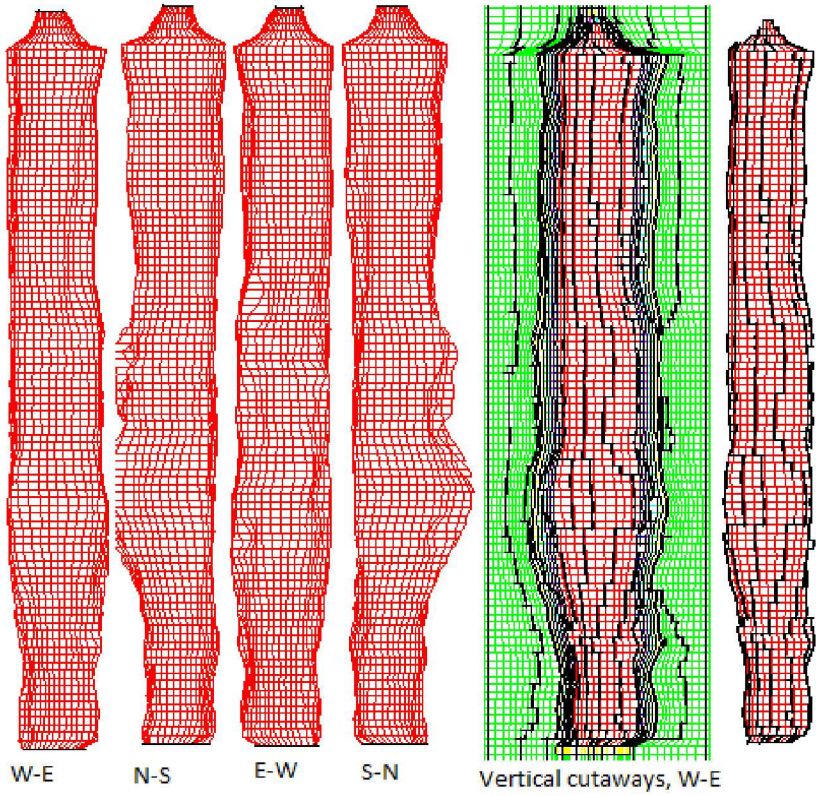

Figure 12. Computational mesh from sonar geometries for BM-103.

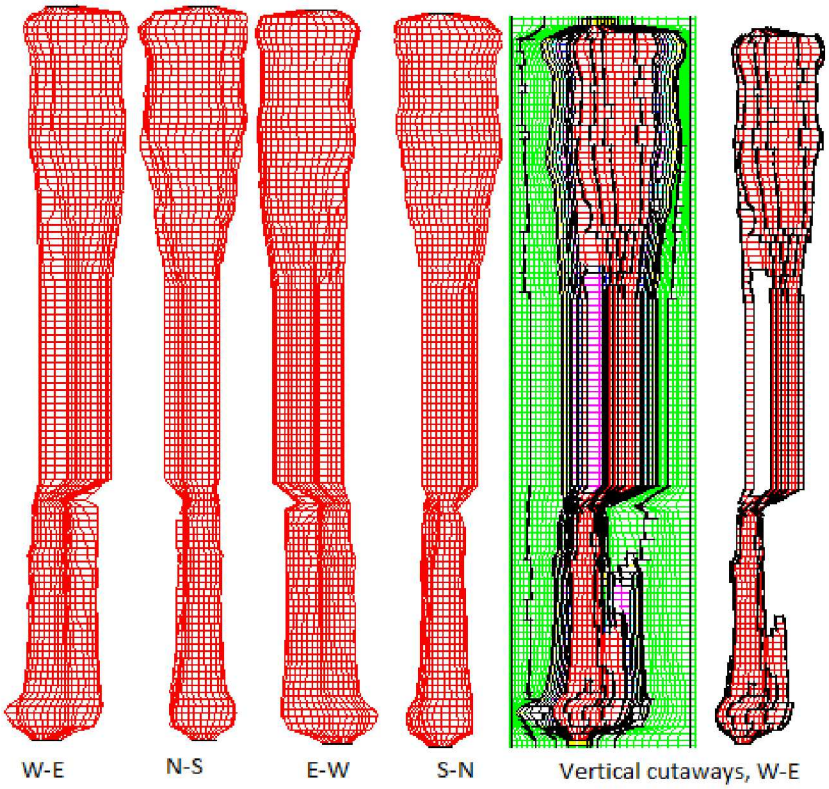

Figure 13. Computational mesh from sonar geometries for BM-105

3.3 COMPUTATIONAL AND MATERIAL MODELS

This analysis utilized the high-performance finite element code Adagio (SIERRA Team, 2010, 2011; Arguello et al., 2012), a three-dimensional finite element program developed by Sandia National Laboratories, and designed to solve large quasi-static nonlinear mechanics problems. Adagio is written for parallel computing environments, and its solvers allow for scalable solutions of very large problems. Adagio uses the SIERRA Framework, which allows for coupling with other SIERRA Mechanics codes. The development of the SIERRA Mechanics code suite has been funded by the Department of Energy (DOE) Advanced Simulation and Computing (ASC) program for nearly twenty years (Edwards and Stewart, 2001). The goal is development of massively parallel multi-physics capabilities to support the Sandia engineering sciences mission. SIERRA Mechanics was designed and developed from its inception to run on the latest, most sophisticated, massively parallel computing hardware. It has the capability to span the hardware range from a single workstation to computer systems with thousands of processors. The foundation of SIERRA Mechanics is the SIERRA toolkit, which provides finite element application-code services such as: (1) mesh and field data management, both parallel and distributed; (2) transfer operators for mapping field variables from one mechanics application to another; (3) a solution controller for code coupling; and (4) included third party libraries (e.g., solver libraries, communications package, etc.). The SIERRA Mechanics code suite comprises application codes that address specific physics regimes. Adagio is used for solid mechanics problems by solving quasi-static, large deformation, large strain behavior of nonlinear solids in three dimensions. Adagio has Sandia-developed (i.e., proprietary) technology for solving solid mechanics problems, that involves matrix-free iterative solution algorithms for efficient solution of extremely large and highly nonlinear problems. This advanced technology is especially well-suited for scalable implementation on massively parallel computers.

The multi-mechanism deformation (M-D) model of salt creep (Munson & Dawson, 1979, 1982, & 1984) is currently being used for modeling salt creep behavior. The M-D model is a rigorous mathematical description of both transient and steady-state creep phenomena, and provides a realistic model of the transient behavior of salt under pressure change conditions such as a workover. This constitutive model considers three well-recognized fundamental features of a creeping material: a steady-state creep rate, a transient strain limit, and both a work-hardening and recovery time rate of change (*i.e.* curvature). Because of the highly non-linear nature of the curvature of the transient strain response, this model has been difficult to integrate in a fully three-dimensional calculation for a model with hundreds of thousands of elements. Many published papers exist presenting two-dimensional calculations using the M-D model, but three-dimensional, large-scale simulations have been more difficult due to the model's high nonlinearity. Sobolik et al. (2010) documents the integration algorithm enhancements of the M-D model that allow it to be utilized for large-scale three-dimensional calculations.

The following discussion of the M-D model was provided by Jim Bean for inclusion in Sobolik et al. (2010). The MD model mathematically represents the primary and secondary creep behavior of salt due to dislocations under relatively low temperatures (compared to the melting temperature) and low to moderate stresses which are typical of mining and storage cavern

operations. Three micromechanical mechanisms, determined from deformation mechanism maps (Munson, 1979), are represented in the model: 1) a dislocation climb mechanism active at high temperatures and low stresses, 2) an empirically-observed mechanism active at low temperatures and low stresses, and 3) a dislocation slip mechanism active at high stresses. These creep mechanisms are assumed to act such that the total steady state creep rate $\dot{\varepsilon}_s$ can be written as the sum of the individual mechanism strain rates.

$$\dot{\varepsilon}_s = \sum_{i=1}^{3} \dot{\varepsilon}_{s_i} \tag{1}$$

The influence of temperature on the creep strain rate is included through an Arrhenius term. The steady state creep strain rates for the first and second mechanisms are identical in form and are implemented using a power law model while the third mechanism (dislocation slip) is represented using an Eyring type model.

$$\dot{\varepsilon}_{s_1} = A_1 \left(\frac{\sigma_{eq}}{G} \right)^{n_1} e^{\frac{-Q_1}{RT}} \tag{2}$$

$$\dot{\varepsilon}_{s_2} = A_2 \left(\frac{\sigma_{eq}}{G} \right)^{n_2} e^{\frac{-Q_2}{RT}} \tag{3}$$

$$\dot{\varepsilon}_{s_3} = \left(B_1 e^{-Q_1/RT} + B_2 e^{-Q_2/RT} \right) \sinh\left[q \left(\frac{\sigma_{eq} - \sigma_0}{G} \right) \right] H\left(\sigma_{eq} - \sigma_0 \right) \tag{4}$$

where:

σ_{eq}	equivalent stress
T	temperature (absolute)
G	shear modulus
A_1, A_2, B_1, B_2	structure factors
Q_1, Q_2	activation energies
R	universal gas constant
q	activation volume
σ_0	stress limit
H	Heaviside function with argument $(\sigma_{eq} - \sigma_0)$

From the definition of the Heaviside function, the third mechanism is only active when the equivalent stress exceeds the specified value of the stress limit σ_0. The equivalent stress appearing in these equations is taken to be the Tresca stress (Munson, et al., 1989). The Tresca stress can be written in terms of the maximum and minimum principal stresses σ_1 and σ_3 respectively ($\sigma_1 \geq \sigma_2 \geq \sigma_3$). Alternatively, the Tresca stress may be written as a function of the

Lode angle ψ and the second invariant J_2 of the deviatoric stress tensor **s** (whose components are s_{ij}).

$$\sigma_{eq} = \sigma_1 - \sigma_3 = 2\cos\psi\sqrt{J_2} \tag{5}$$

The Lode angle is dependent on both the second and third invariant J_3 of the deviatoric stress tensor s_{ij}.

$$\psi = \frac{1}{3}\sin^{-1}\left[\frac{-3\sqrt{3}J_3}{2J_2^{3/2}}\right] \qquad -\frac{\pi}{6} \le \psi \le \frac{\pi}{6} \tag{6}$$

$$J_2 = \frac{1}{2}s_{ij}s_{ji} \tag{7}$$

$$J_3 = \frac{1}{3}s_{ij}s_{jk}s_{ki} \tag{8}$$

The kinetic equation used in the MD model is given by Equation 9 where F is a function which accounts for transient creep effects and $\dot{\varepsilon}_s$ is the steady state dislocation creep strain rate defined by Equation 1.

$$\dot{\varepsilon}_{eq} = F\dot{\varepsilon}_s \tag{9}$$

The function F has three branches: a work hardening branch ($F > 1$), an equilibrium branch ($F = 1$), and a recovery branch ($F < 1$).

$$F = \begin{cases} \exp\left[\Delta\left(1-\dfrac{\zeta}{\varepsilon_t^f}\right)^2\right] & \zeta < \varepsilon_t^f \quad \text{Transient Branch} \\ 1 & \zeta = \varepsilon_t^f \quad \text{Equilibrium Branch} \\ \exp\left[-\delta\left(1-\dfrac{\zeta}{\varepsilon_t^f}\right)^2\right] & \zeta > \varepsilon_t^f \quad \text{Recovery Branch} \end{cases} \tag{10}$$

The choice of the particular branch depends on the transient strain limit ε_t^f and the internal variable ζ. The transient strain limit is defined by Equation 11 where K_0, c, and m are material parameters, T is the absolute temperature, and G is the shear modulus.

$$\varepsilon_t^f = K_0 e^{cT} \left(\frac{\sigma_{eq}}{G} \right)^m \tag{11}$$

The internal variable ζ, appearing in the calculation of the function *F,* is obtained by integration of the evolution equation

$$\dot{\zeta} = (F - 1)\dot{s} \tag{12}$$

Δ and δ, appearing in Equation 10, are the work hardening and recovery parameters and are given by Equations 13 and 14 respectively. In these equations α, β, α_r, and β_r are material parameters. Typically, the recovery parameter δ is taken to be constant (i.e. $\delta = \alpha_r$).

$$\Delta = \alpha + \beta \log\left(\frac{\sigma_{eq}}{\mu} \right) \tag{13}$$

$$\delta = \alpha_r + \beta_r \log\left(\frac{\sigma_{eq}}{\mu} \right) \tag{14}$$

If only the steady state creep response is of interest then the transient and recovery branches may be effectively turned off by setting $\alpha = 0$, $\beta = 0$, $\alpha_\gamma = 0$, $\beta_\gamma = 0$. The MD model can be further simplified to that of a power law creep model by setting the appropriate structure factors and activation energies to zero.

For three dimensional states of stress the components of the creep strain rate tensor are generalized (Fossum et al., 1988) as

$$\dot{\varepsilon}_{ij}^c = \dot{\varepsilon}_{eq} \frac{\partial \sigma_{eq}}{\partial \sigma_{ij}} \tag{15}$$

Using the Tresca stress (Eq. 5) as the equivalent stress in this form means the creep strains are purely deviatoric ($\dot{\varepsilon}_{ij}^c = \dot{\varepsilon}_{ij}^c$ since $\dot{\varepsilon}_{kk}^c = 0$) and that all volume change is elastic as defined though the bulk modulus *K* (i.e. $\varepsilon_{kk} = \sigma_{kk} / 3K$). Therefore Equation 15 becomes

$$\dot{\varepsilon}_{ij} = \dot{\varepsilon}_{eq} \frac{\partial \sigma_{eq}}{\partial \sigma_{ij}} = \dot{\varepsilon}_{eq} N_{ij} \tag{16}$$

Including the bulk and shear moduli, which are both assumed constant, there are a total of 19 parameters used to define the MD model.

3.4 MATERIAL PROPERTIES OF SALT – SELECTION BY COMPARISON WITH DATA

It is desirable in large geomehcanical calculations to use salt properties that have been obtained through both laboratory experiments and through corroboration with measured field data such as cavern closure and surface subsidence. Laboratory values for SPR salts in Munson (1998) identify the West Hackberry and Big Hill salts as "soft" salts, and Bayou Choctaw and Bryan Mound as "hard" salts. For the Bryan Mound site, these properties were further calibrated by numerical analysis to match the estimated cavern closure and measured surface subsidence rates at the site (Sobolik and Ehgartner, 2009, 2012a, 2012b; Sobolik, 2010; Sobolik & Lord, 2014). The starting point for the property values for Bryan Mound were developed from laboratory tests on core reported in Munson (1998); that property set for the M-D model is listed in Table 2. The development of the property sets used in the Sandia dome-scale model have advanced from the use of the power law creep model (essentially Equation 3) to the M-D model, from modeling overall properties for "hard" and "soft" sections of the Bryan Mound salt dome, and to estimation of "cavern-specific" creep properties in the regions immediately surrounding each cavern. The necessity for developing improved M-D property sets for Bryan Mound is explained by the wide variability in the estimated cavern closure rates for each cavern. Table 3 lists the average cavern closure rates for each Bryan Mound cavern over three different time periods. Note that for the Phase 2 caverns (101-116) which have similar geometries and depths, there is an order of magnitude difference in closure rates. These closure rates are derived from the wellhead pressure histories from each cavern, from which the code CAVEMAN (Ballard & Ehgartner, 2000; Ehgartner, 2004 & 2009) calculates a cumulative loss in cavern volume. The ultimate goal of the modeler is to develop a set of M-D model properties, along with the given model, that produces predicted cavern volume loss and surface subsidence as close to estimated/measured values as possible.

Table 2. M-D Model mechanical properties published for Bryan Mound salt in Munson (1998)

Property	Bryan Mound salt properties
Density, lb/ft^3	144 (2300 kg/m^3)
Elastic modulus, lb/ft^2	648×10^6 (31.0 GPa)
Shear modulus G, lb/ft^2	259×10^6 (12.4 GPa)
Poisson's ratio	0.25
Primary Creep Constant A_1, sec^{-1}	1.445×10^{22}
Exponent n_1	5.5
Q_1, cal/mol	25000
Secondary Creep Constant A_2, sec^{-1}	1.667×10^{12}
Exponent n_2	5.0
Q_2, cal/mol	10000
B_1, sec^{-1}	1.049×10^6
B_2, sec^{-1}	0.523×10^{-2}
σ_0, , lb/ft^2	429×10^3 (20.57 MPa)
q	5335
m	3.0
K_0	6.275×10^5
c (1/R) (0.009198/1.8)	0.00511
α	-17.37
β	-7.738
δ	0.58

Table 3. Cavern closure rates at Bryan Mound as determined from CAVEMAN.

	Cavern closure rates estimated from CAVEMAN, BBL/year		
Cavern	1/1/1990-7/26/2016	1/1/1990-12/31/2007	1/1/2008-7/26/2016
BM1	2622	2422	3041
BM2	284	274	307
BM4	11775	11390	12458
BM5	22275	25581	15298
BM101	9579	8918	10960
BM102	7616	6018	10960
BM103	17581	16508	19690
BM104	10304	10482	9888
BM105	6306	6943	4950
BM106	19635	18204	22602
BM107	12126	14168	7820
BM108	9235	10542	6437
BM109	15090	16064	13016
BM110	7753	7270	8241
BM111	9531	8259	12148
BM112	16105	14902	18482
BM113	16218	16253	16061
BM114	23479	25007	20249
BM115	25028	24943	25310
BM116	10370	10417	10249

Previous Bryan Mound analyses cited above had greater success in matching measured surface subsidence than for estimated cavern volume loss. Because of the importance in understanding the effects of salt creep on the borehole casings in the salt, and on cavern integrity, it was decided to place greater priority on matching the cavern volume loss behavior in the simulations. A series of different simulations was run with the computational mesh described herein, and with the known pressure histories through 7/26/2016, while varying two specific property values. The values that were modified were the secondary creep coefficient A_2 (Equation 3) and the transient coefficient K_0 (Equation 11). The creep coefficient A_2 was chosen because that creep mechanism is the dominant steady-state creep mechanism. The transient coefficient K_0 was chosen to capture the large volume change that occurs during a workover. Multipliers were applied to these two coefficients from the Munson values in Table 2 to vary the creep properties; all other values listed in Table 2 were unchanged. Because of the large amount of time to run a simulation through the existing life of the facility, only four such simulations were performed. The set of multipliers that produced the best agreement with the estimated cavern volume closure data are listed in Table 4. The M-D creep properties represented by these values were used to obtain the results presented throughout this report. For most of the caverns, the same set of properties were used for the six skin layers that surround the cavern and the cylinder that surrounds those skin layers (see Figures 12 and 13). However, for a few caverns the cylinder was given different properties, to balance out the effect of workovers from one cavern affecting closure in adjacent caverns The results shown in Section 4 will depict a better agreement with the CAVEMAN derived data, but at a cost of the overprediction of surface subsidence. An updated

verification of the methodology CAVEMAN uses to calculate cumulative cavern volume change from wellhead pressure data will be performed in the near future, and this will give better insight into the appropriateness of the coefficient multipliers in Table 4 used for these analyses.

Table 4. Multpliers applied to Secondary Creep Coefficient A_2, Transient Coefficient K_0 for each dome or cavern region, for analyses in this report

Salt of Cavern Region	A_2 multiplier	K_0 multiplier	Cylinder
Hard salt	2.3	1.0	--
Soft salt	24.0	1.0	--
BM-1 (leach layers + cylinder)	6.0	1.0	Same
BM-2 (leach layers + cylinder)	19.08	1.0	Same
BM-3 (leach layers + cylinder)	19.08	1.0	Same
BM-4 (leach layers + cylinder)	31.0	1.0	Same
BM-5 (leach layers + cylinder)	1.94	1.0	Same
BM-101 (leach layers + cylinder)	1.89	0.1	Same
BM-102 (leach layers + cylinder)	5.0	0.1	Same
BM-103 (leach layers + cylinder)	50.0	0.5	Same
BM-104 (leach layers + cylinder)	1.46	2.0	Hard salt
BM-105 (leach layers + cylinder)	1.85	1.0	Same
BM-106 (leach layers + cylinder)	25.	1.0	Same
BM-107 (leach layers + cylinder)	1.5	1.0	Hard salt
BM-108 (leach layers + cylinder)	0.14	1.5	Hard salt
BM-109 (leach layers + cylinder)	7.0	1.0	Same
BM-110 (leach layers + cylinder)	1.5	1.0	Same
BM-111 (leach layers + cylinder)	20.0	0.16	Same
BM-112 (leach layers + cylinder)	1.5	1.5	Cavern 109
BM-113 (leach layers + cylinder)	40.0	1.0	Soft salt
BM-114 (leach layers + cylinder)	200.0	1.0	Soft salt
BM-115 (leach layers + cylinder)	200.0	1.0	Soft salt
BM-116 (leach layers + cylinder)	4.36	1.0	Same

3.5 OTHER MATERIAL PROPERTIES

The surface overburden layer, which mostly comprises sand and sandstone, is considered isotropic and elastic, and has no assumed failure criteria. The caprock layer, consisting of anhydrite and limestone with some gypsum, is also assumed to be elastic for this analysis. As described earlier, several well casing failures at the Bryan Mound site indicate that the caprock has been significantly altered due to steam-injection sulfur mining from the early 1900s, which both compromised the mechanical integrity of the caprock and left a significant increase in temperature that still remains. The caprock was also known to be significantly rubblized in various locations. Therefore, the caprock does not behave in a homogeneous, elastic manner in its entirety. For this analysis, though, it is modeled as an elastic medium to allow for an easier comparison with previous analyses, and to determine the potential effect of subsidence over Cavern 3 may have on the site. The sandstone surrounding the salt dome is assumed to be elastic

(Lama and Vutukuri, 1978). Mechanical properties of each of these geologic materials used in the present analysis are listed in Table 5.

Table 5. Material properties of other geologic materials.

Parameters	Units	Overburden	Caprock	Sandstone
Density	lbm/ft^3	117.	156.	133.6
Young's Modulus	lb/ft^2	2.09×10^6	146×10^6	153×10^6
Poisson's Ratio		0.33	0.29	0.33

The sulfur mining in the caprock at Bryan Mound in the early 20th century was performed using the Frasch extraction method, for which superheated steam at 320°F was injected into the caprock to draw out sulfur, in a mostly molten form with some SO_2 and H_2SO_4. This steam remained in situ within the caprock, and the heat was contained in the caprock and conducted into the underlying salt dome. Borehole temperature logs were taken for each cavern between 2001 and 2003. These vertical temperature profiles are plotted in Figure 14. The caverns with the lowest maximum temperatures, Caverns 111, 114, 115, and 116, all lie on the periphery of the cavern field. The red linear plot in Figure 14 represents an in situ profile based on an independent borehole temperature log in salt at cavern depth; this linear profile has been used in the past for modeling exercises. However, a curve fit based on the average measured temperatures was used for this analysis; this curve fit is also shown in Figure 14. Cavern 3 is located at depths between 1560 and 1680 feet, which puts it in a region where the measured borehole temperature is a few degrees higher than the linear in situ salt temperature. The salt above the cavern at the salt-caprock interface may be at temperatures 30°F higher than the in situ temperature. The curve fit temperature profile for caverns located below 2000 feet of depth is nearly identical to the in situ linear equation used for Sobolik and Ehgartner (2009), so the different temperature profile is expected to have a negligible effect on predicted cavern closures and surface subsidence for those caverns. The curve fit temperature profile used for Bryan Mound is described by the following equations:

For depth z between 0 and 360 feet, $T = 72 + 0.09647z$
For depth z between 360 and 1040 feet, $T = -2.478E\text{-}4z^2 + 0.3857z$
For depth z between 1040 and 2000 feet, $T = -3.387E\text{-}5z^2 - 0.1179z + 219.05$
For depth z greater than 2000 feet, $T = 118.7 + 0.0153*(z-2000)$

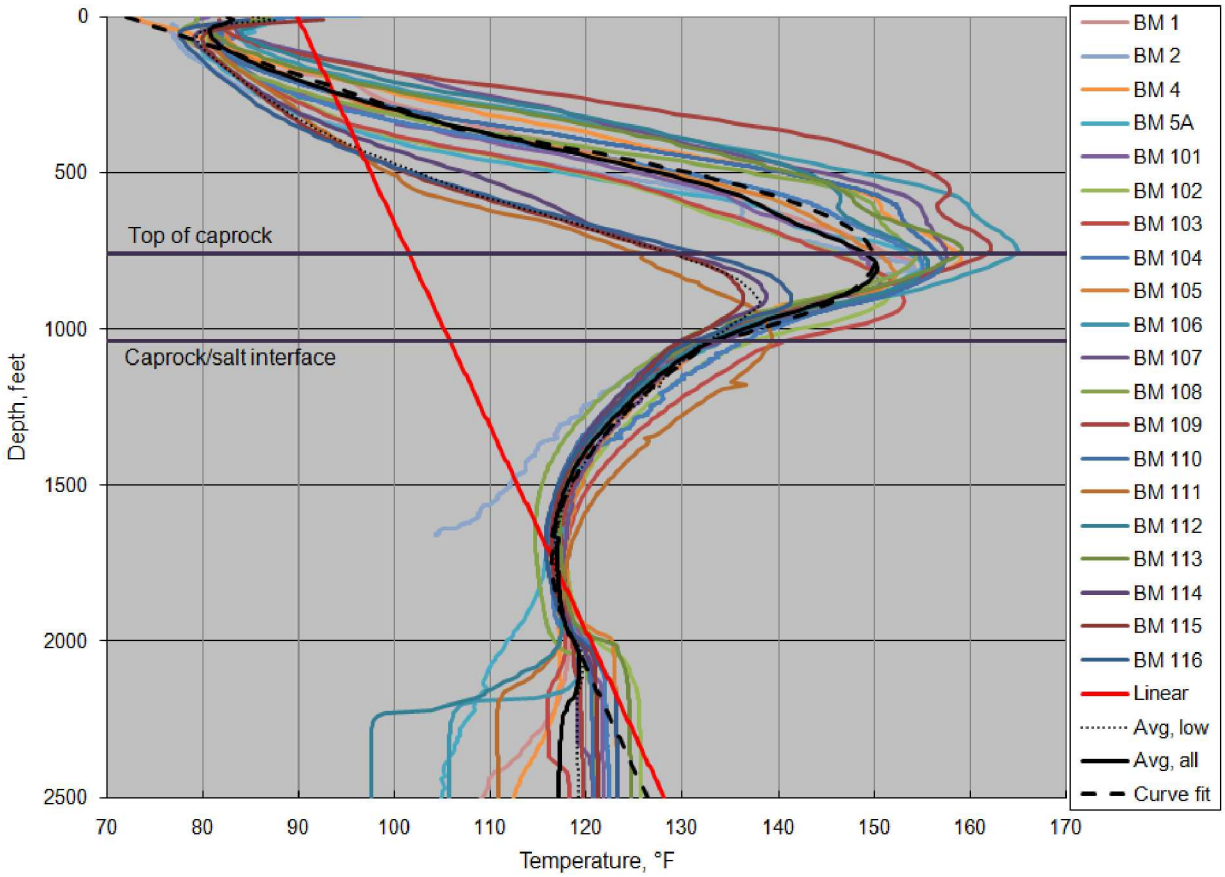

Figure 14. Bryan Mound temperature profiles, including measurements from each borehole, average values and curve fits.

3.6 DAMAGE CRITERIA

The damage factor criterion (analogous to a safety factor) has been developed as a linear function of the onset of dilatant damage as a function of the hydrostatic pressure (Van Sambeek et al., 1993). Dilatancy is considered the onset of damage to rock resulting in increases in permeability. Dilatant damage in salt typically occurs at the stress state at which a rock begins microfracturing, causing an increase in the rock volume. Dilatant criteria typically relate two stress invariants: the mean stress invariant I_1 (equal to three times the mean stress) and the square root of the stress deviator invariant J_2, or $\sqrt{J_2}$ (a measure of the overall deviatoric or dilatant shear stress). (By convention, tensile normal stresses are positive, and compressive normal stresses are negative, hence the sign nomenclature in the following equations.) The dilatant criterion chosen here is the equation typically used from Van Sambeek et al. (1993),

$$\sqrt{J_2} = -0.27 I_1 . \qquad (17)$$

The damage criterion defines a linear relationship between I_1 and $\sqrt{J_2}$, and such a linear relationship has been established from many suites of laboratory tests on WIPP, SPR, and other salt samples. This criterion was applied during post-processing of the analyses, using predicted

stress states. A damage factor (safety factor) index was created (*SF*) by normalizing I_1 by the given criterion:

$$SF_{VS} = \frac{-0.27 I_1}{\sqrt{J_2}} \tag{18}$$

Several earlier publications define that the damage factor *SF* indicates damage when *SF*<1, and failure when *SF*<0.6. In previous studies, values of *SF*<1.5 have been categorized as cautionary due to unknown localized heterogeneities in the salt that cannot be captured in these finite element calculations. This report will use these damage thresholds.

In addition to the damage criterion based on deviatoric stresses, the onset of tensile stresses is also used as an indicator of fracture formation in the salt. Salt, like most geomaterials, has a very low tensile strength. Engineering literature spanning several decades list tensile strength values of salt ranging from 1 MPa to 3 MPa. For the purposes of this report, a value of 1 MPa (145 psi, or 20900 psf) will be assumed.

4. RESULTS

The historical and predicted future performance of the Bryan Mound caverns was evaluated on the basis of four design factors: cavern volume closure, surface subsidence, axial well strain in the salt and caprock, and dilatant and tensile stress damage to the salt surrounding the caverns. In the first two sections, the results of the analyses during the historical operations period will be compared to Bryan Mound data for cavern volume closure and surface subsidence, to evaluate the effectiveness of the chosen material property sets. Then predicted behavior through five drawdown cycles will be discussed. The following sections will examine the predicted axial well strains induced by salt creep, and the potential development of tensile and dilatant stresses in the salt surrounding the caverns. The discussion of tension and dilatancy will also be used to briefly describe how these analyses are used to determine the number of available drawdowns for each cavern.

When examining the results described in the following sections, it is important to remember that these calculations were performed with a specific set of assumptions. Even though the computational model has several options built into it to examine various geomechanical aspects of the Bryan Mound site, a single 80-year simulation takes 4-6 weeks to run even on high performance computing machines. Therefore, this analysis considers one set of assumptions; other assumptions will be considered in future model applications. The primary assumptions for this set of calculations include:

- The use of CAVEMAN-generated cavern volume closure (Ballard and Ehgartner, 2000) corresponding to historical wellhead pressures; there has been some recent discussions about the accuracy of the calculated volume changes, and a future task will reevaluate, revalidate, and probably reprogram the CAVEMAN algorithm to produce values more in line with recorded fluid exchanges in the caverns.
- A low but constant brine pressure in Cavern 3, equivalent to approximately 25% of the in situ lithostatic pressure in the surrounding salt (equivalent to a residual brine head in the sealed borehole beginning near the top of the caprock). Previous Bryan Mound analyses investigated the enhanced surface subsidence over Cavern 3 by instituting a gradually decreasing pressure in the cavern that leveled at a low pressure near 10% of the in situ lithostatic pressure (equivalent to the top of the brine head located at the salt/caprock interface). For this first run of the new model, the higher pressure was chosen to evaluate the sensitivity of surface subsidence to pressures within the abandoned cavern; different approaches are planned to be used in the future.
- The undamaged and damaged caprock were given same material model and properties. It was shown in previous Bryan Mound analyses (Sobolik 2010) that a damaged caprock can have significant effects on the distribution of shear and normal stresses throughout the caprock, as undamaged sections of caprock will take on greater loads to compensate for the weakened mined areas. Because of the length of computation time for a full model run, this analysis does not utilize that capability; future analyses will investigate the effects of the damaged caprock.
- These analyses were performed assuming that Cavern 2 would still be used as an oil storage cavern. During the time the calculations were run, the decision was made to fill

Cavern 2 with brine and decommission its use for oil storage. The model was kept as is, and its results should still be useful for projecting the cavern's future behavior.

4.1 CAVERN VOLUME CLOSURE

The volume of the caverns decreases as the salts creeps. The only active measurements of cavern volume occur during sonar measurements of the caverns, and these are performed once every few years. The daily evolution of cavern volume change must be derived from knowledge about the creep rate of the salt under its given stress and temperature conditions, the compressibility of the fluid, and fluid pressure at any point in the cavern, which is a function of the pressure at the wellhead. The program CAVEMAN (Ballard & Ehgartner, 2000; Ehgartner, 2004 & 2009) is used to calculate the daily change to cavern volume, based on the parameters previously stated. These values are not true measurments, but will be referred to as measured data throughout this report. Figures 15 and 16 plot comparisons of the predicted cavern volume closure history and that measured for the caverns in the hard salt; the values are percentage change in volume normalized by the original volume of each cavern. Figure 17 compares predicted and measured values for the caverns in the soft salt. The step changes in the cavern volume closure correspond to workovers when the wellhead pressure was lowered to near zero; these times induce the greatest change in cavern volume as the differential stress in the salt is greatest and the strain rate due to creep is correspondingly highest (see Equation 3). In general, the predicted behavior of the caverns matches the measured behavior farily well, particularly the rates of volume change during the normal operations phases. The instances where large discrepancies occur tend to during the workovers, and also very early in the time period plotted. The comparisons shown here are significantly better than those published in earlier Bryan Mound studies, particularly Sobolik & Ehgartner (2009). The reasons for the closer predictions include better cavern-specific creep coefficients, and the use of the actual cavern wellhead pressure histores. The caverns in the soft salt, primarily 114, 115, 113, and 106, have the highest average cavern closure rates, ranging from 0.15 to 0.23%/year. Caverns 1, 2, and 5 experience the least closure because they are shallower than the other caverns, thus avoiding the higher stress differential between cavern pressure and in situ stress experienced at greater depths. The maximum average closure rate for these caverns is 0.04%/year. In the hard salt, Cavern 103 has the highest average closure rate at about 0.13%/year. The site average closure rate for Bryan Mound is 0.096%/year, which is leess than half for West Hackberry at 0.22%/year. This point substantiates the notion that, on average, Bryan Mound is a harder salt, even though it has significant localized heterogeneities. For all the cylinderically-shaped caverns, the majority of the volume loss occurs near the bottom of these caverns because of the greater stress differential at lower depths.

Figures 18 through 20 shpw projections of the volume losses for the Bryan Mound caverns through five drawdowns. The percentage losses are normalized to the volumes of the caverns after each successive drawdown; this allows for a continuous sense of how much volume is lost to salt creep even as volume is gained during drawdown-induced leaching. The most significant observation to be made from these figures is that the cavern volume loss rate is expected to increase as the thickness of the pillars between caverns are reduced by the leaching process. This decerease in pillar thickness and corresponding increase in creep rate will have an effect on cavern integrity in the future.

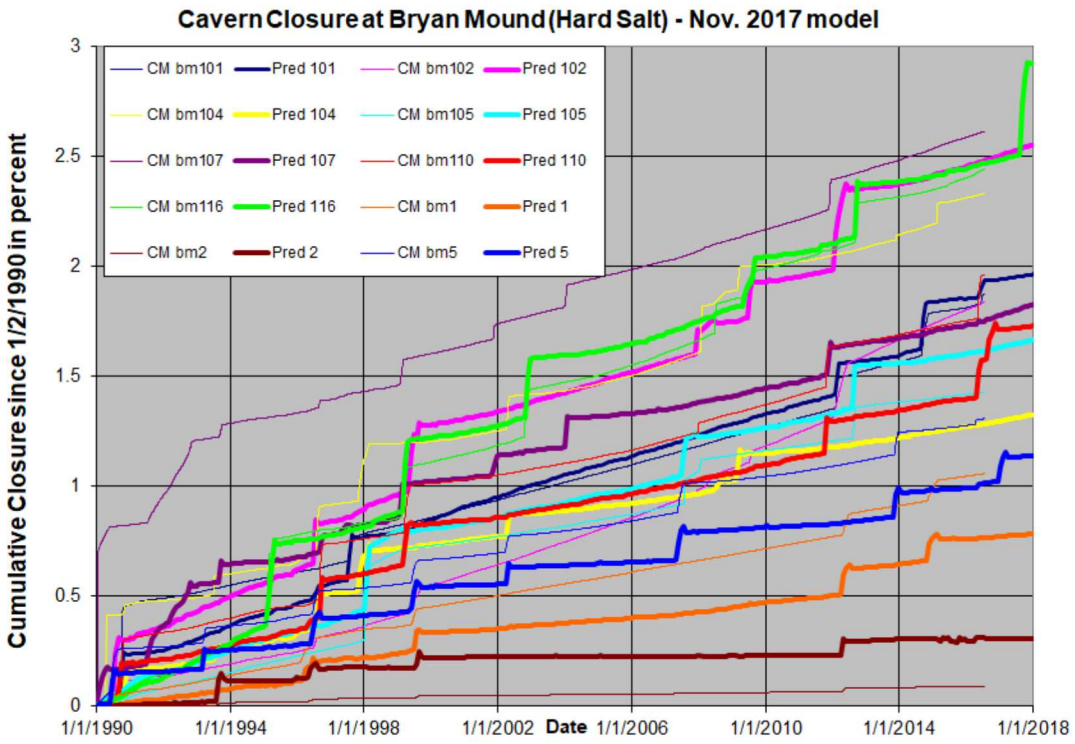

Figure 15. Comparison of measured (CAVEMAN – CM) and predicted (computational model) cumulative cavern closures for caverns in the hard salt at Bryan Mound.

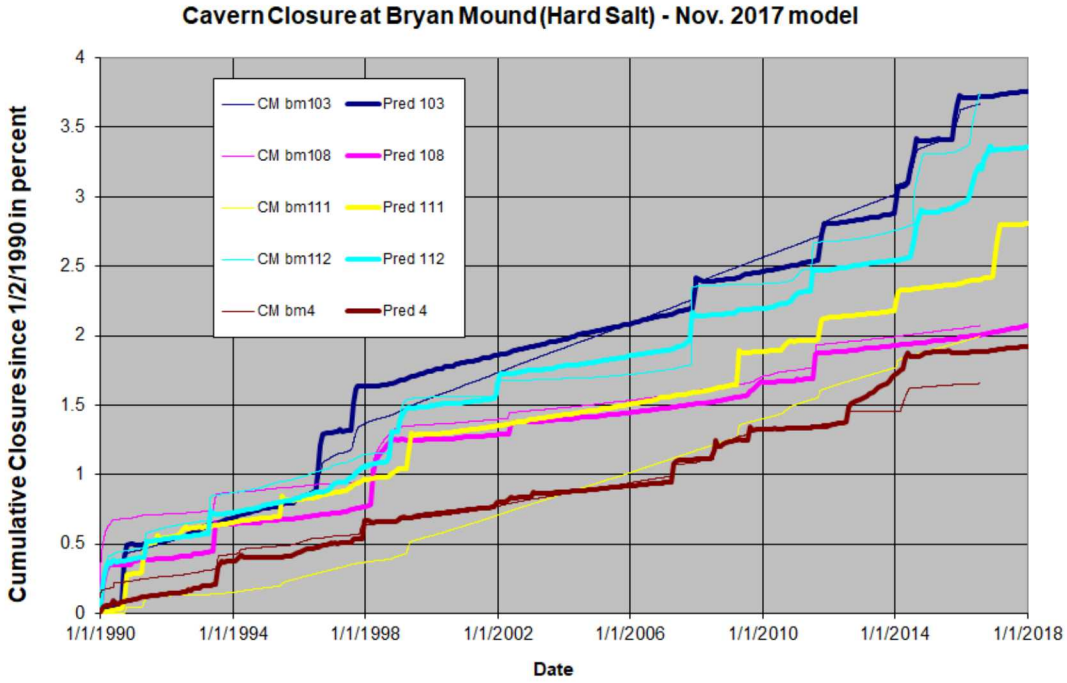

Figure 16. Comparison of measured (CAVEMAN – CM) and predicted (computational model) cumulative cavern closures for caverns in the hard salt at Bryan Mound (Part 2).

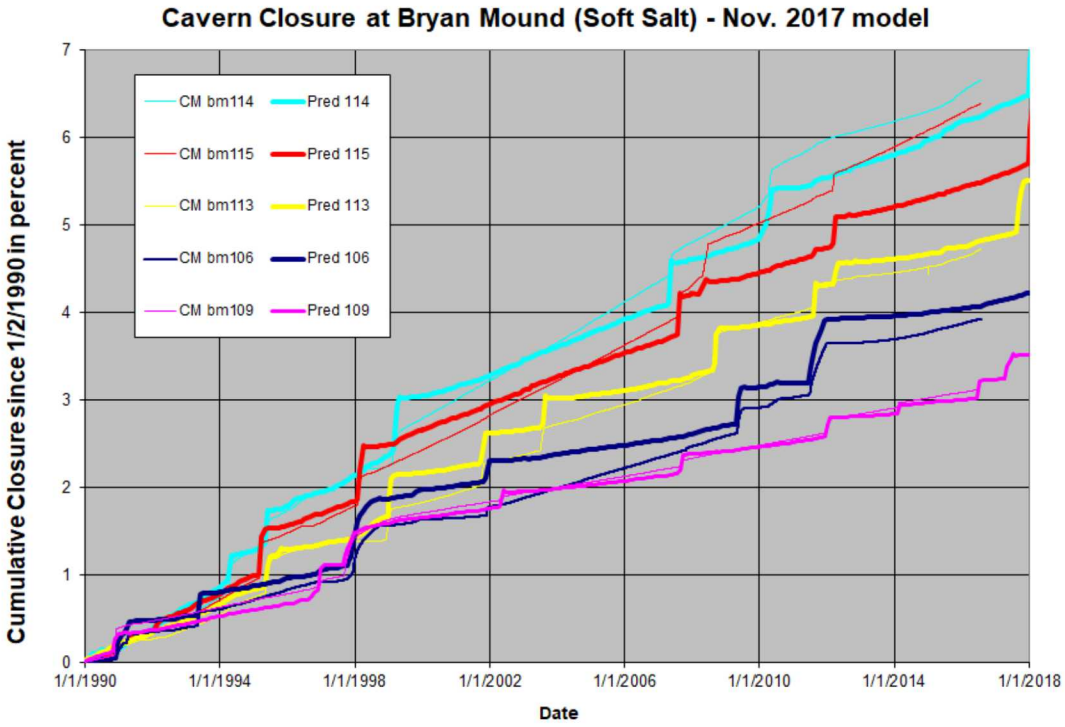

Figure 17. Comparison of measured (CAVEMAN – CM) and predicted (computational model) cumulative cavern closures for caverns in the soft salt at Bryan Mound.

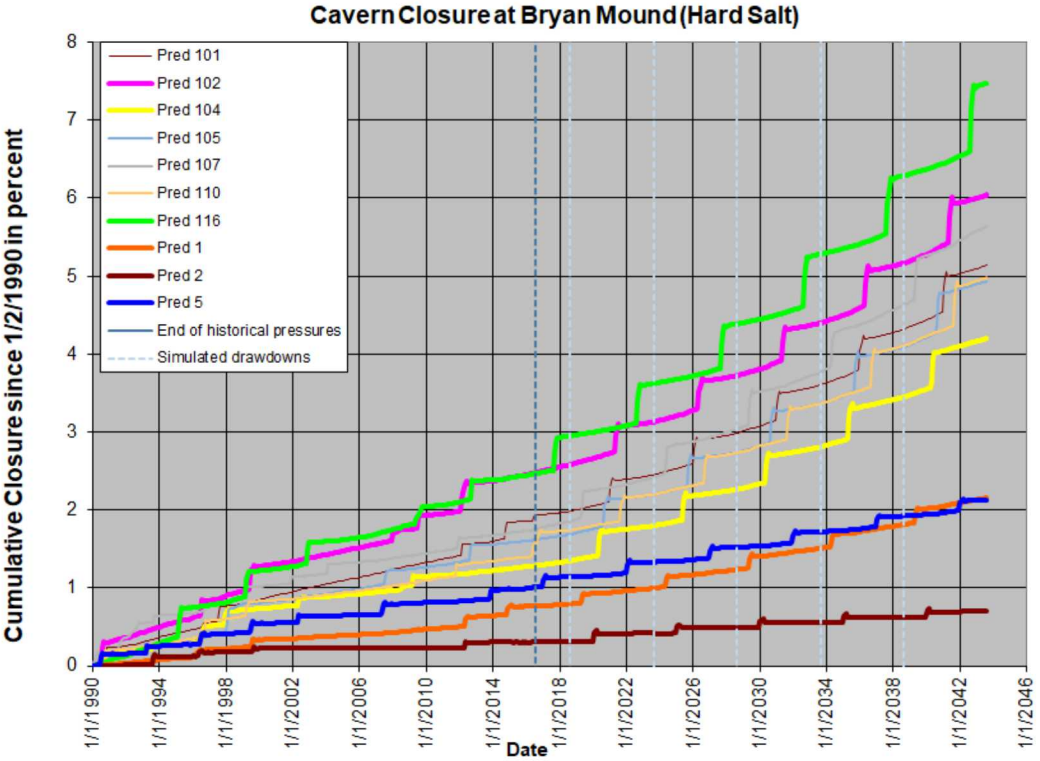

Figure 18. Predicted cumulative cavern closures for caverns in the hard salt at Bryan Mound through five simulated drawdowns.

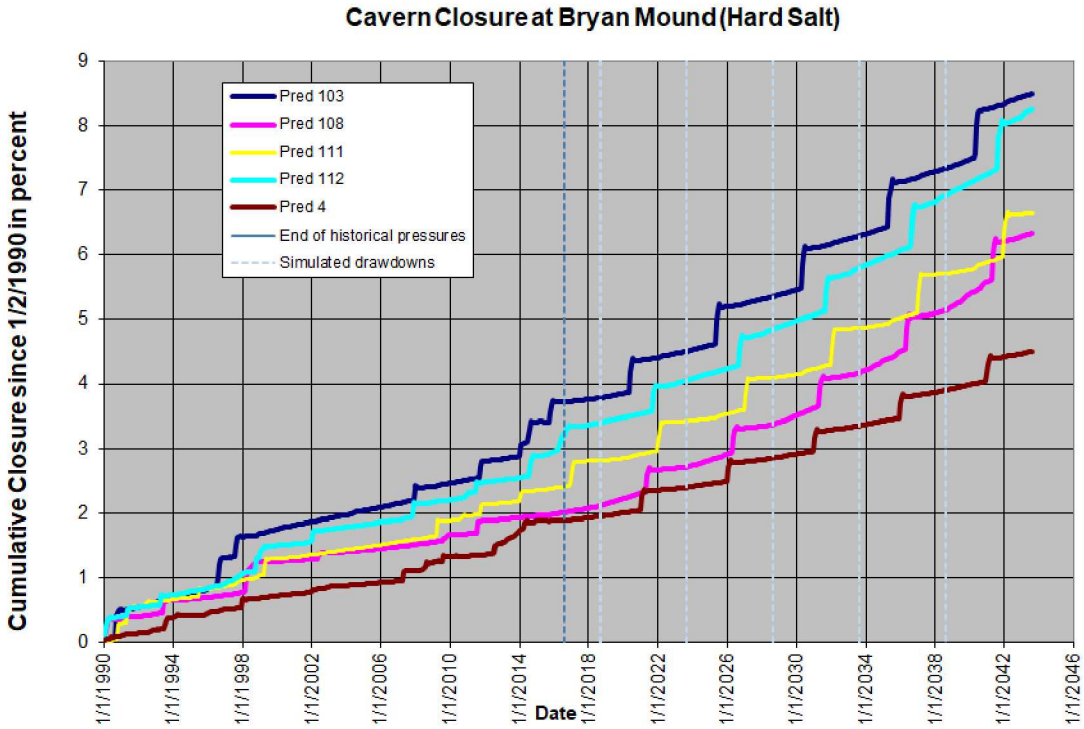

Figure 19. Predicted cumulative cavern closures for caverns in the hard salt at Bryan Mound through five simulated drawdowns (Part 2).

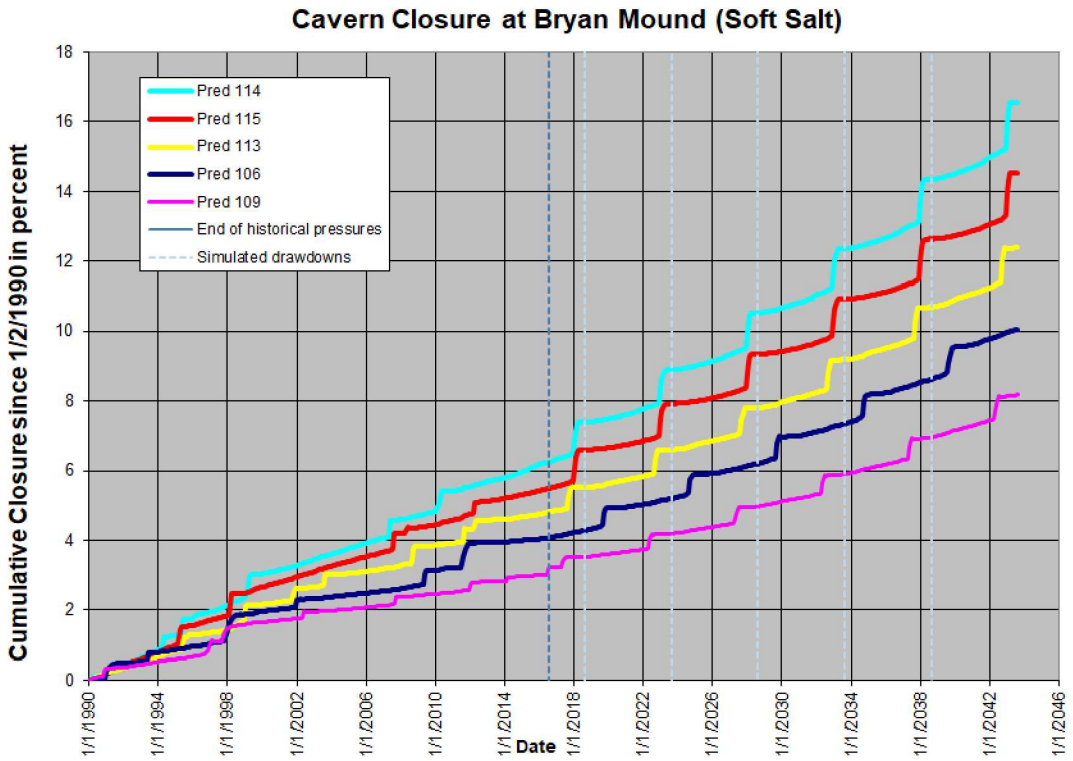

Figure 20. Predicted cumulative cavern closures for caverns in the soft salt at Bryan Mound through five simulated drawdowns.

4.2 SURFACE SUBSIDENCE

The issue of surface subsidence is an important design and operations factor for surface facilities, especially for those located in flood prone areas, but subsidence also results in horizontal ground strains that can damage buildings, pipelines, and other infrastrusture. The SPR is currently nearly 40 years old and the life of the SPR may extend well into this century depending upon a number of factors, including oil consumption, import dependency, and geopolitical instability.

The history of subsidence measurements at Bryan Mound has two consistent themes: 1) there have been many erratic or erroneous readings over the years due to measurements methods, use of markers instead of monuments, unreliable reference point data, which have complicated the understanding of long-term trends over the Bryan Mound site; 2) one undeniable trend, though, is that the surface above abandoned Cavern 3 is subsiding at a greater rate than the rest of the site. The enhanced surface subsidence over Cavern 3 is significant for two reasons. The first is that the point of maximum subsidence over an oil storage site would normally be expected to be over the center of the site, as the integrative effects of creep in normally operating caverns propagate to the surface. The fact that the subsidence over Cavern 3 is greater indicates that the cavern is creeping faster than normal due to a low cavern pressure and/or loss of fluid into the formation. The second reason is the several key surface facilities are located above or very near the footprint of Cavern 3, including the main access road to the SPR offices over the middle of the cavern, four oil and brine storage tanks on the northern perimeter, and Caverns 115 and 116 near its southern perimeter. These themes developed from Bryan Mound surface subsidence measurements have been observed and documented throughout the years in the following figures: Figure 21 (Lord, 2009 and 2010), which plots the measured subsidence rates over the Bryan Mound site based on the site-wide measurements taken in January 2007 and April 2009; Figure 22 (Lord, 2010), which plots the subsidence rates over the site based on site-wide measurements taken in April 2009 and October 2010; and Figure 23 (Moriarty, 2017), which plots time-averaged subsidence rates from 2010 through 2016. All figures indicate an increase in subsidence rate over Cavern 3 as compared to the rest of the Bryan Mound site, although the later plots show smaller differences. In 2013, a GPS measurement unit was installed at the original Cavern 3 wellhead location, and tiltmeters were installed there and at the northern and southern perimeter of the Cavern 3 footprint. Figure 24 shows the measured subsidence over Cavern 3 from the GPS instrumentation. These figures, and others in Moriarty (2017), indicate the overall subsidence rate has slowed in the past five years, however, the area over Bryan Mound Cavern 3 is still experiencing the highest subsidence at approximately 0.04 ft./yr (based on the surveyed subsidence measurements). This area has experienced more than a foot of subsidence since the surveys began in 1988. The GPS at the site shows a general subsidence rate of 0.023 ft./yr. with some annual periodic behavior; this number differs slightly from the number derived from survey data (Moriarty, 2017). Because of the erratic data sets, and the variability subsidence rate values coming from different times and different data sets, it is difficult to develop a direct comparison between measured subsidence data and predicted values rom the geomechanical model.

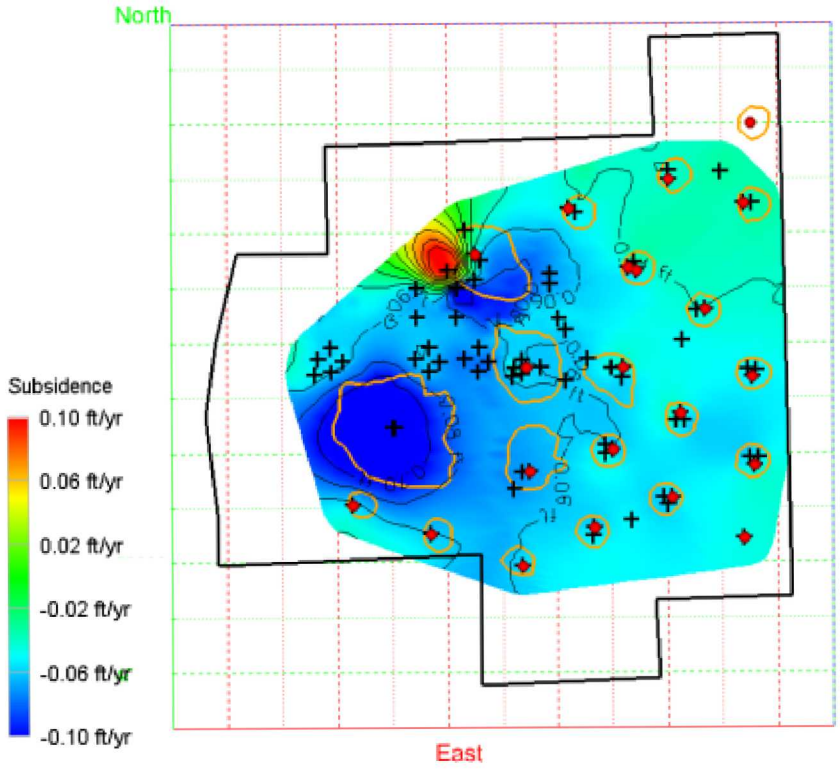

Figure 21. Contour plot of subsidence rates (ft/yr) from January 2007 to April 2009 (Lord, 2009).

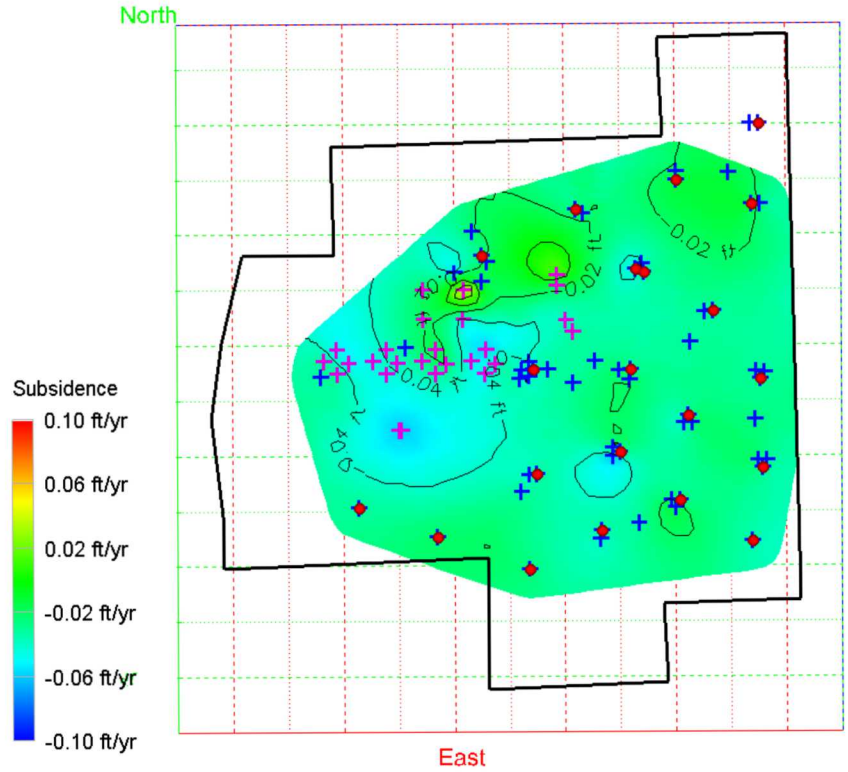

Figure 22. Contour plot of subsidence rates (ft/yr) from April 2009 to Oct. 2010 (Lord, 2010).

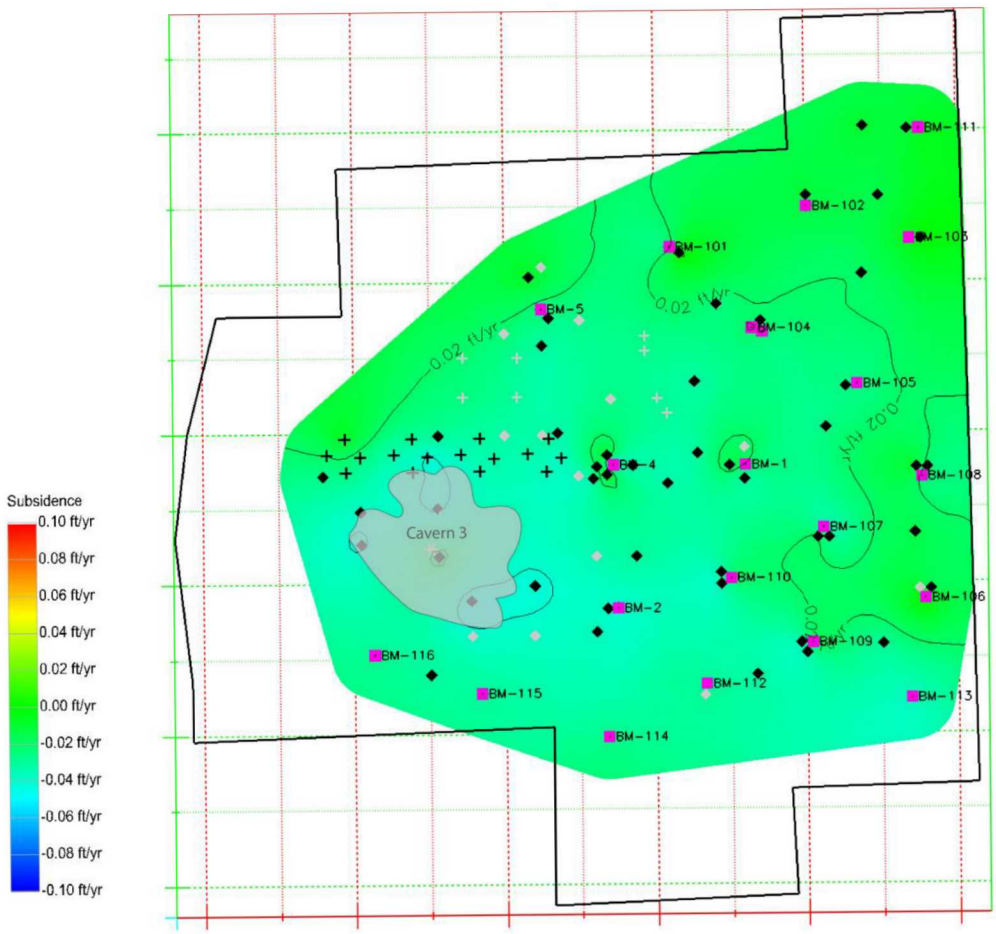

Figure 23. Historical subsidence rates at Bryan Mound from October 2010 to July 2016. Diamonds represent survey monuments while crosses represent survey markers.

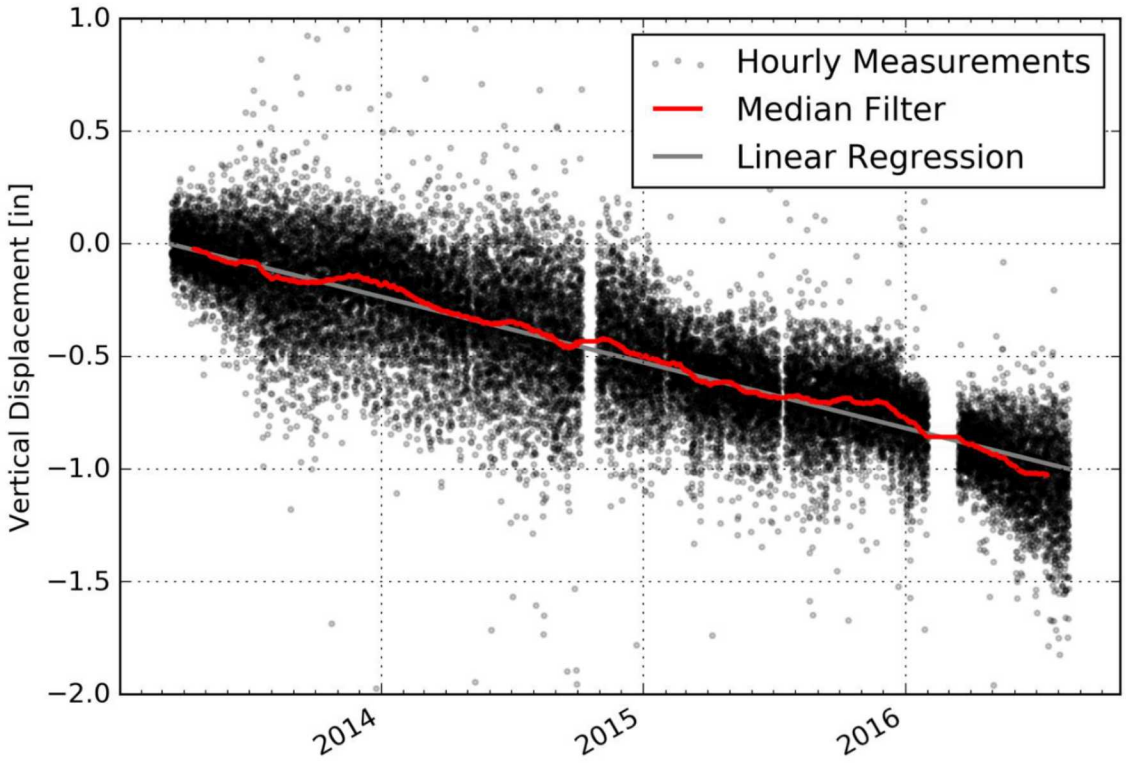

Figure 24. Hourly GPS measurements of vertical displacement seen at the Bryan Mound GPS with both a median filter (red) and a linear regression, or best fit line (grey), applied to the hourly data (Moriarty, 2017).

Figures 25 through 27 compares the surveyed surface subsidence measurements over the caverns to the predicted values from the geomechanical model: Figure 25 shows Caverns 101-108, Figure 26 Caverns 109-116, and Figure 27 Caverns 1-5. (The dashed lines are predictions, and the lines with points are measured data). The immediate observation is that the predicted subsidence values are generally larger than the measured values. Some of the difference is due to some discrepancies in the early-year data, which display some erratic behavior. In later years, if the slopes or rates of change of the curves are examined, the discrepancies are not as great as they might appear, although they still exist. These results differ from the previous Bryan Mound models, for which the predictions for surface subsidence matched data much better than the predictions for cavern volume closure. There are several potential reasons for this discrepancy: the derived cavern volume closure values may be inaccurate; the properties for the M-D model still do not truly reflect the overall behavior of the salt; the existence of anhydrite in large quantities in the salt dome may cause less overall change in the dome geometry than the model currently predicts; and the properties used for the caprock and overburden may be overly high regarding elastic deformation.

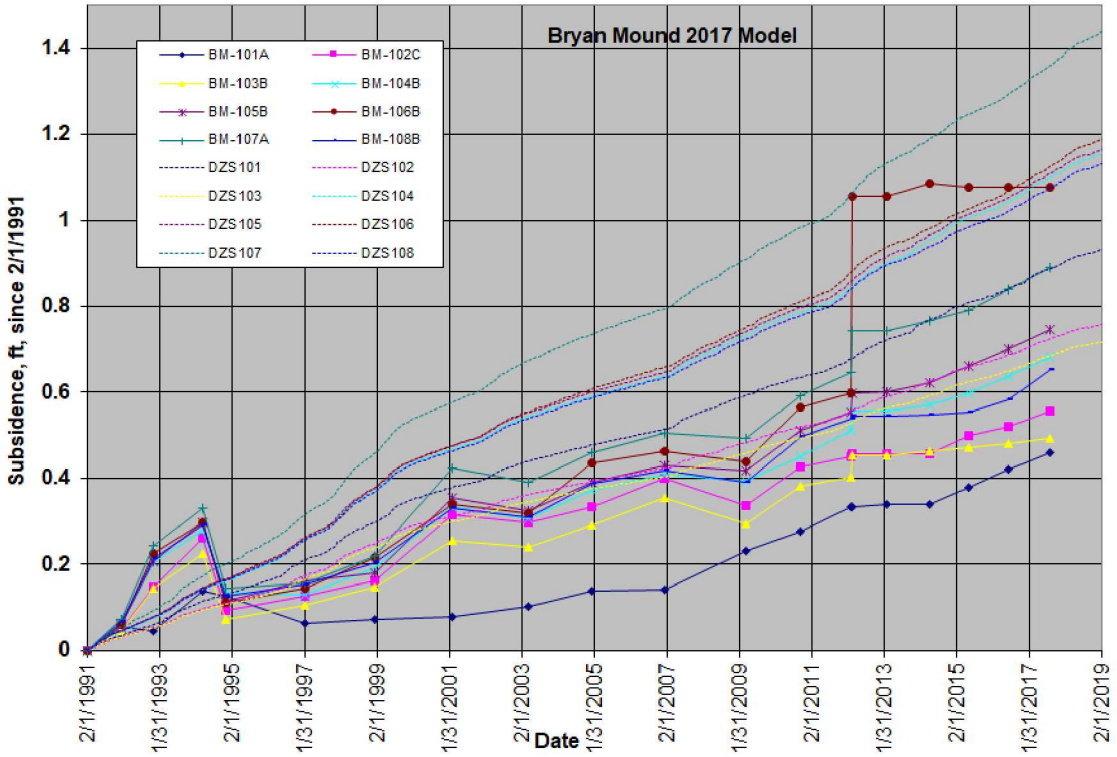

Figure 25. Comparison of measured and predicted cumulative surface subsidence for Bryan Mound Caverns 101-108.

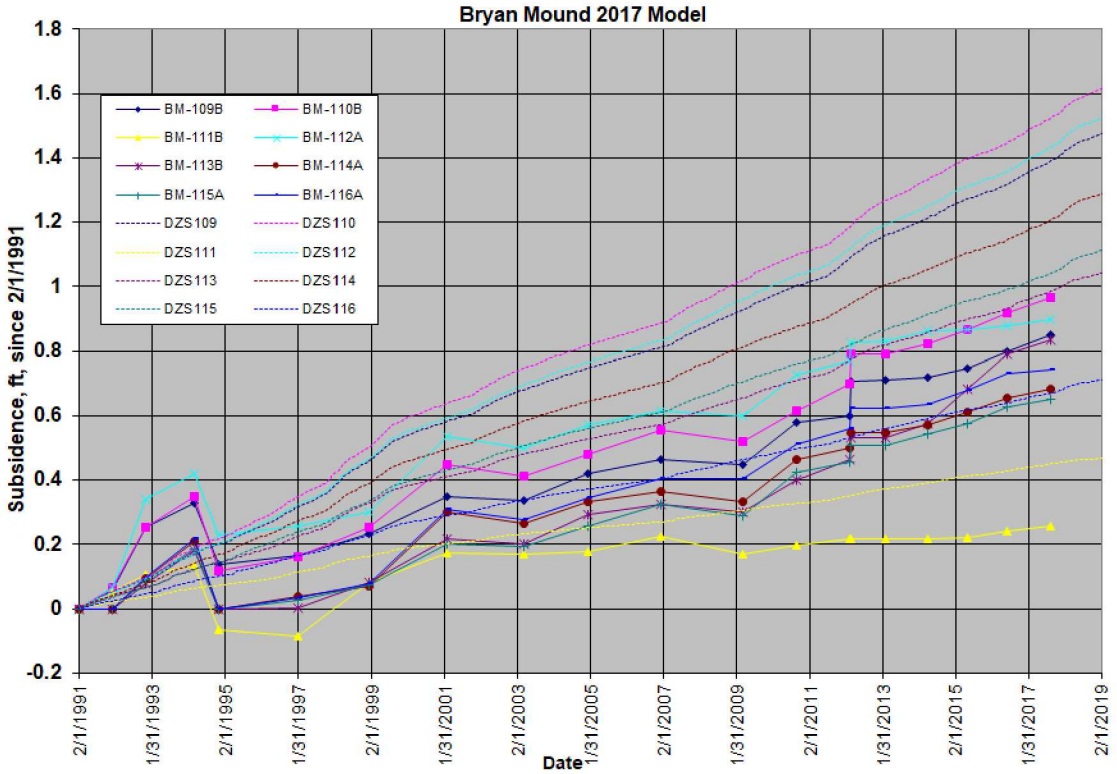

Figure 26. Comparison of measured and predicted cumulative surface subsidence for Bryan Mound Caverns 109-116.

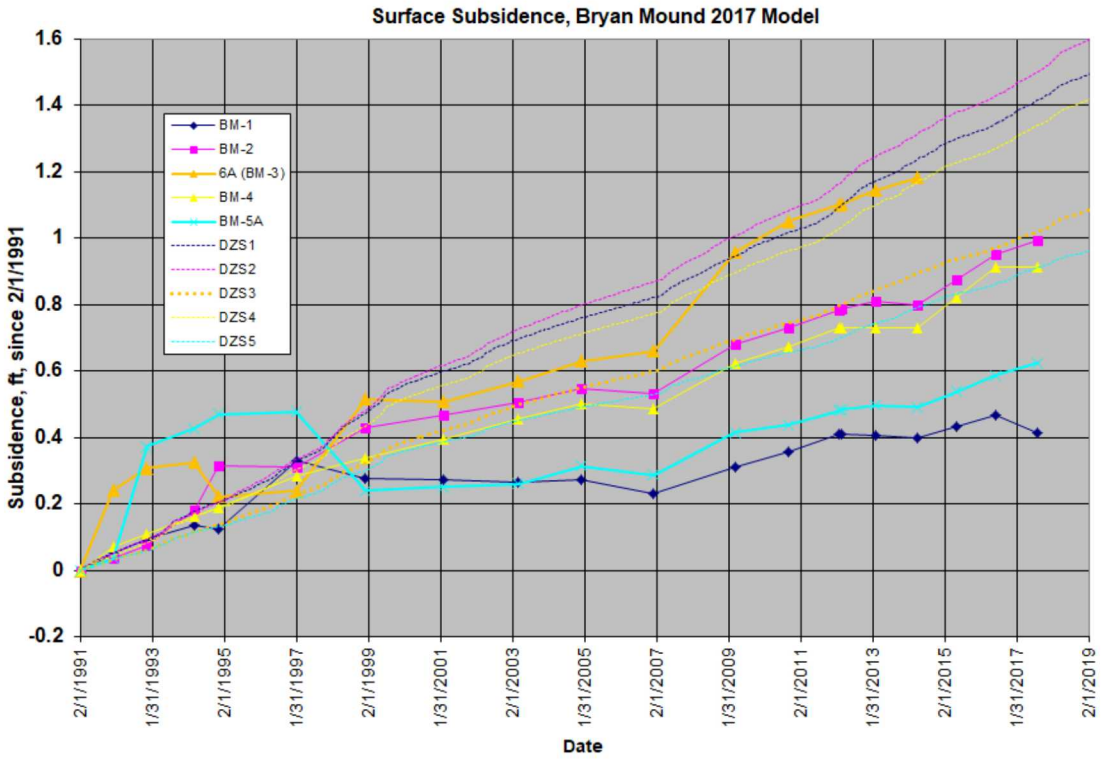

Figure 27. Comparison of measured and predicted cumulative surface subsidence for Bryan Mound Caverns 1-5.

One of the other important observations from Figure 27 is the predicted behavior of the subsidence over Cavern 3; in this figure, this predicted subsidence is not greater than that over the rest of the caverns. This does not correspond with the data shown in Figure 27, or in Figures 21-23, which consistently show the subsidence over Cavern 3 as being the greatest throughout the entire site. The results of prior Bryan Mound geomechanical analyses (Sobolik & Ehgartner, 2012a; Sobolik & Lord, 2014), shown in Figure 28 where the largest subsidence rate is over Cavern 3, led to the hypothesis that the greater subsidence over Cavern 3 was caused by brine in the cavern being compressed by creep-induced closure, causing it to move up the borehole and into the caprock. If this scenario is correct, that would imply that an active brine head of only about 400 feet exists above the top of the cavern. The pressure boundary condition applied to Cavern 3 in the earlier analyses approximates this condition. For the current calculations, a somewhat larger brine head is assumed, going up to near or above the top of the caprock; this increases the simulated pressure in the cavern, but is still significantly less than a typical borehole filled with fluid all the way to the surface. Figure 29 shows predicted subsidence rates for the current analysis, and may be compared to Figure 28; the current calculation predicts the maximum subsidence rates over the center of the site. These results lend credence to the hypothesis that there is a low fluid pressure in the cavern, and a leak path for brine to travel from the cavern up unto the caprock, causing the enhanced subsidence over Cavern 3. Future iterations using this geomechanical model will once again use the lower pressures in modeling Cavern 3.

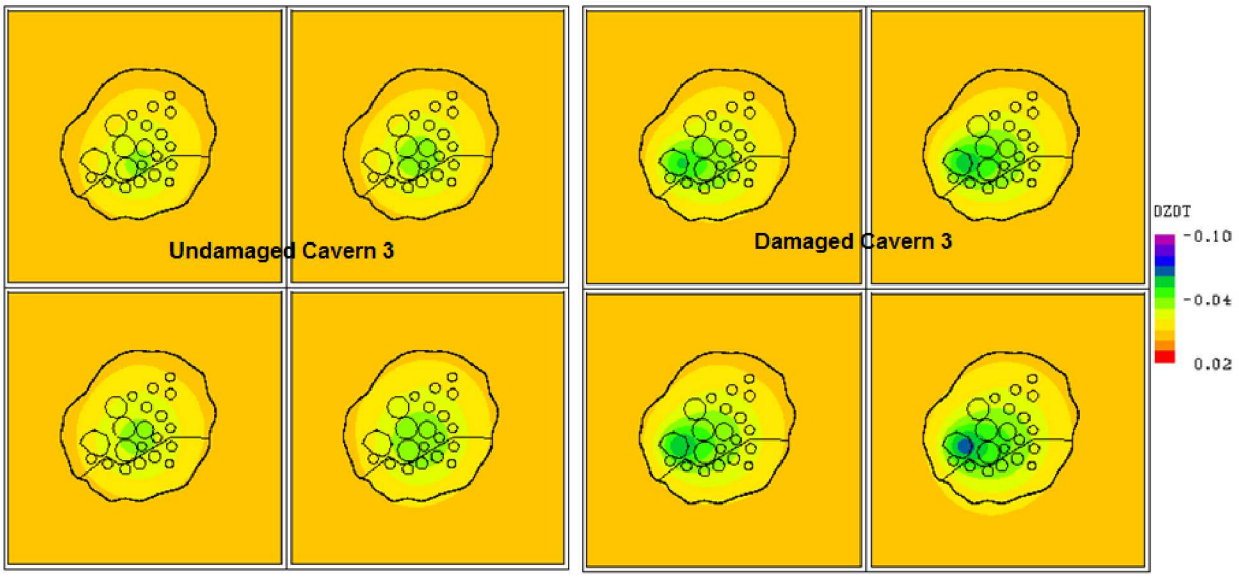

Figure 28. Predicted subsidence rates (ft/yr), 2012 Bryan Mound analysis (Sobolik & Ehgartner, 2012a), undamaged vs. damaged Cavern 3 (times August of 2010, 2011, 2012, 2013).

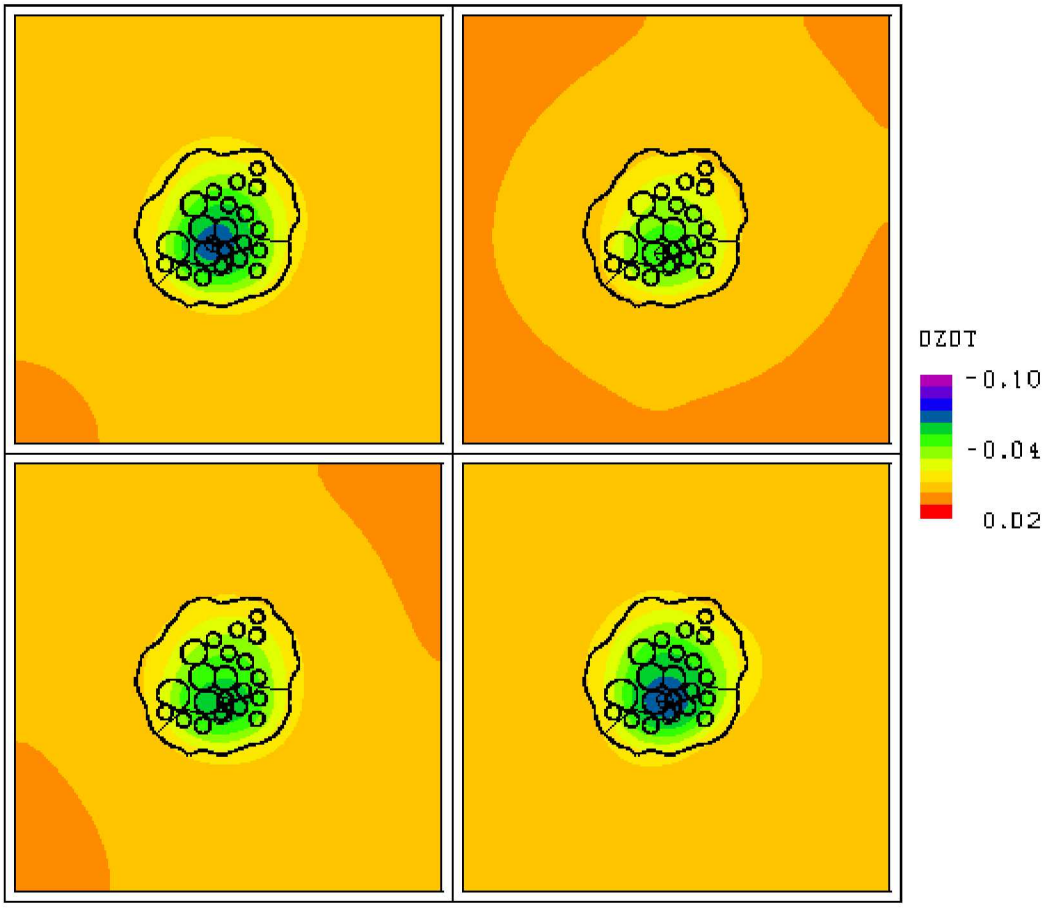

Figure 29. Predicted subsidence rates (ft/yr), current model analysis (times December of 2014, 2015, 2016, 2017).

4.3 AXIAL WELL STRAIN

The physical presence of wells and surface structures are not included in the finite element model, but the potential for ground deformation to damage these structures can be conservatively estimated by assuming that they will deform according to the predicted ground strains. At well locations, subsidence will primarily induce elongation of the axis of the well. Under these conditions, the cemented annulus of the wells may crack forming a horizontal tensile fracture that may extend around the wellbore. This may not result in vertical fluid migration along the casing, but could permit horizontal infiltration into ground waters. This may be a well vulnerability, especially in the caprock, where acidic ground waters may gain access to the steel casing and corrode it. More extensive damage could heavily fracture the cement which could result in a loss of well integrity in that leakage could occur from the cavern along the outside of the casing. Such leakage could result in flow to the surrounding environment, resulting in loss of product. The allowable axial strain for purposes of this report is assumed to be 0.2 millistrains in tension. This would be typical of cement with a compressive strength in the range from 2500 to 5000 psi (Thorton and Lew, 1983). It should also be noted that vertical well strain reduces the collapse resistance of the steel casings. For a typical SPR well located in the caprock, negligible resistance to casing collapse is predicted at 1.6 millistrains, which coincides with the onset of plastic deformation of typical carbon steels used for casings.

Figure 27 plots the axial wellbore strain in salt for all the caverns, as averaged over the entire length of the casing located in the salt. The vast majority of the axial strain occurs in the 100-200 feet above the cavern ceilings, which includes the uncased chimney and can also include the casing shoe and bottom sections of casing. The largest predicted strains occur over caverns with at least one of the following characteristics: they are located in the soft salt south of the boundary shear zone (106, 113, 114, 115); they have larger values for the creep coefficient A_2 as described in Table 4 (2, 4, 103, 106, 111, 113, 114, 115); or they have large roof diameters (2, 4). It is encouraging that none of the caverns is predicted to have axial strains in the salt that exceed the 1.6-millistrain plastic threshold for steel for until several years from now. This minimizes the likelihood of strain-induced casing collapse, but it does not preclude the potential for tension-induced thread-jumping at the casing joints.

An additional observation to be made from Figure 30 concerns the large tensile strains predicted for Caverns 114 and 115. Predictions from the earlier Bryan Mound models predicted well strains for those caverns that indicated that the well casings in the salt would already be well into the plastic strain mode, and may be severely damaged (Sobolik & Ehgartner, 2012a). However, multi-arm caliper measurements from those wells taken within the past several years indicate only small trajectory misalignments and ovalities. The newer predicted behaviors for these caverns, which were probably influenced by increasing the creep coefficients in the surrounding salt and caverns and thus spreading out the deformation over a larger volume, appear to be more representative of what has been observed in the field.

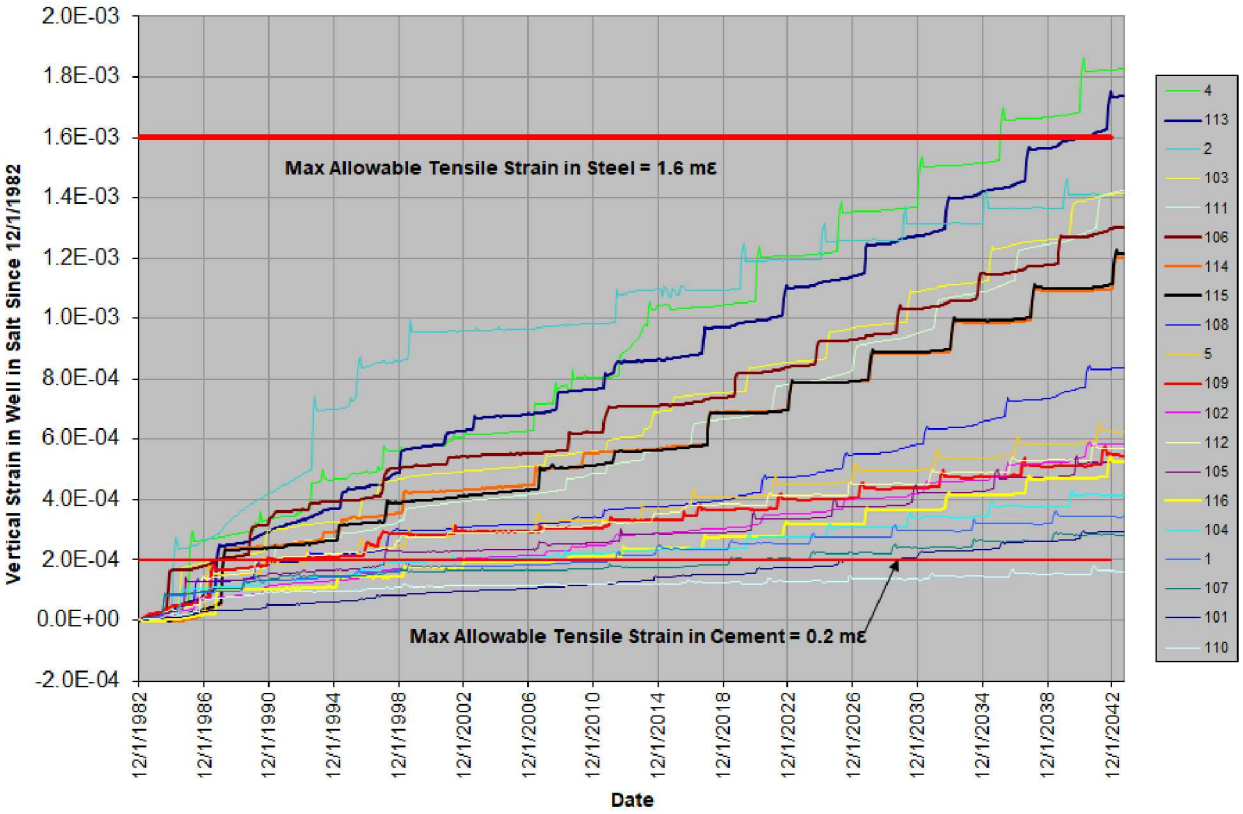

Figure 30. Predicted axial wellbore strain in the salt.

4.4 STRESS-RELATED DAMAGE

There are two ways in which the salt surrounding the caverns can be damaged: by shear-stress induced microfracturing which increases permeability and the potential for crack propagation (commonly called dilatancy), and by tensile stresses which causes salt tensile fracture and crack propagation. A quick way to evaluate the potential for damage is by the use of history plots of the extreme values of damage factor (Equation 18) and maximum principal stress in the salt surrounding the cavern through each of the five leaching operations. As stated previously, lower values for damage factor indicate a higher likelihood for dilatant damage, with values <1.5 considered cautionary, values <1.0 indicating the onset of damage, and values <0.6 indicating failure of the salt, primarily in the form of substantial increase in permeability due to microcracking. In the computational mesh used for these analyses, each cavern is surrounded by a cylinder of salt. The vast majority of the salt in each of the cylinders exists at very low deviatoric stress value, and thus very high values for the damage factor; only in the cavern walls and near vicinity are there sufficient deviatoric stresses to lower the damage factor significantly.

Figure 31 through 33 show the minimum value of the damage factor surrounding each of the caverns as a function of time. In general, the location of the predicted lowest value for damage factor occurs in one of three places in the cavern: the ceiling, where the cavern pressure is much less than the in situ pressure in the salt; the base of the cavern, which can either occur at a cavern "foot" extending around the base of the cavern due to leaching, or an unusual geometry due to the sonar mapping process; and stress concentrations in the side of the cavern due to protuberances wither into or out from the cavern. The downward spikes in the damage factor history plots coincide with actual or projected workovers in that cavern, when the wellhead pressure is dropped to zero causing a commensurate drop in cavern pressure. These low points in the history plots almost always occur in the ceiling, so it is during these times that salt falls are more likely to occur. However, workover-induced salt falls are by themselves a strong indicator of cavern integrity issues, although they have significant potential to damage hanging strings and cause operational issues. It is more important to examine these plots for significant operational periods for which some region of the cavern wall may be experiencing dilatant stresses, when damage factors are less than 1.0. In Figure 31 four caverns display such behavior: 103, 104, 105, and 108. In Figure 32, only Cavern 109 exhibits long-term dilatant behavior, and in Figure 33, Caverns 2, 4, and 5 do so. Caverns 2, 4, and 5 have a much higher diameter-to-height ratio than Caverns 101-116, so it is not surprising that they exhibit higher potential for dilatant conditions associated with workovers (typically in the ceiling, and for the case of Cavern 5, also in the neck between its upper and lower lobes). For Caverns 103 and 105, whose meshes are plotted in Figures 12 and 13, the low values of damage factor occur near the protuberances near the lower middle of the cavern, where stress concentrations would be expected to occur. Caverns 104, 108, and 109 have similar asymmetries in their geometries where these conditions are predicted to occur.

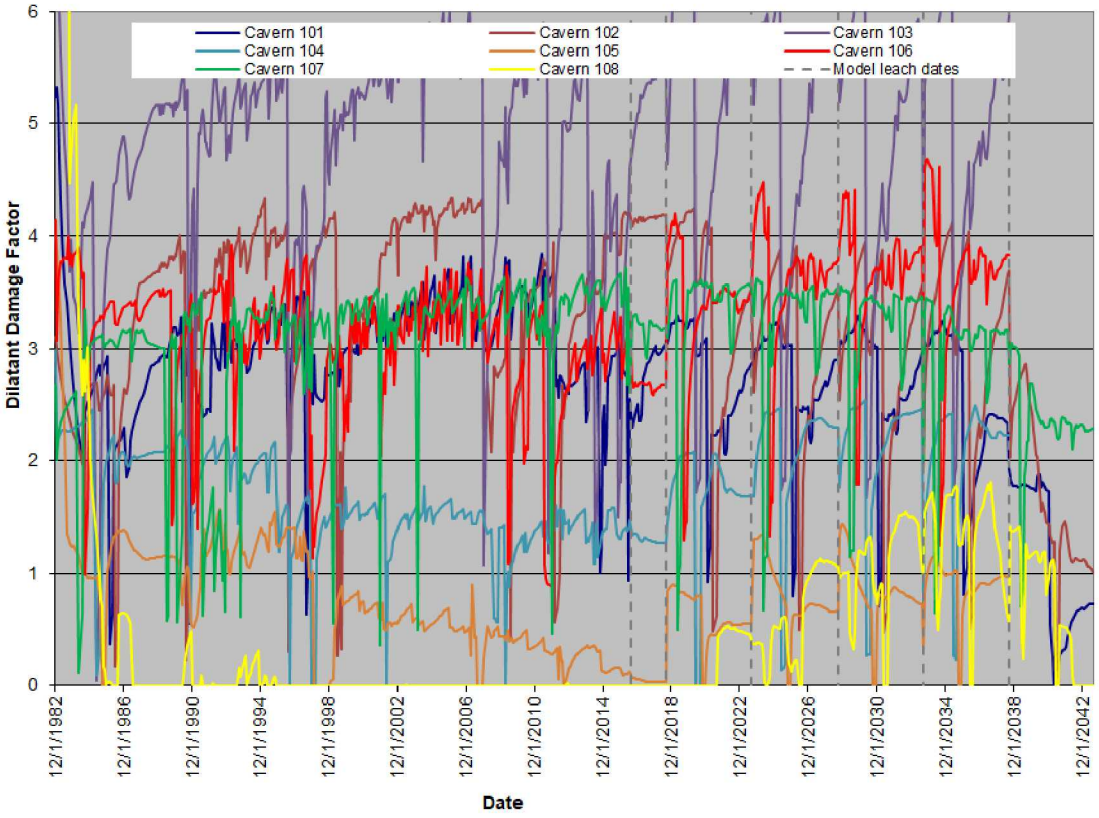

Figure 31. Predicted minimum damage factors for caverns near Caverns 101-108.

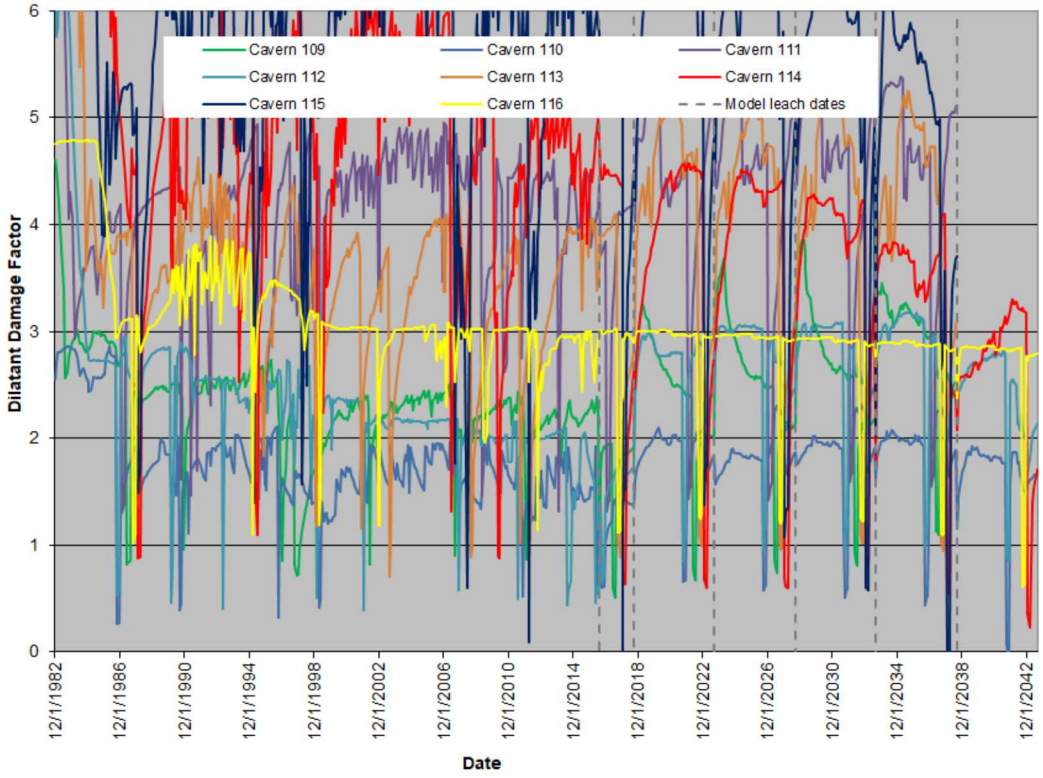

Figure 32. Predicted minimum damage factors for caverns near Caverns 109-116.

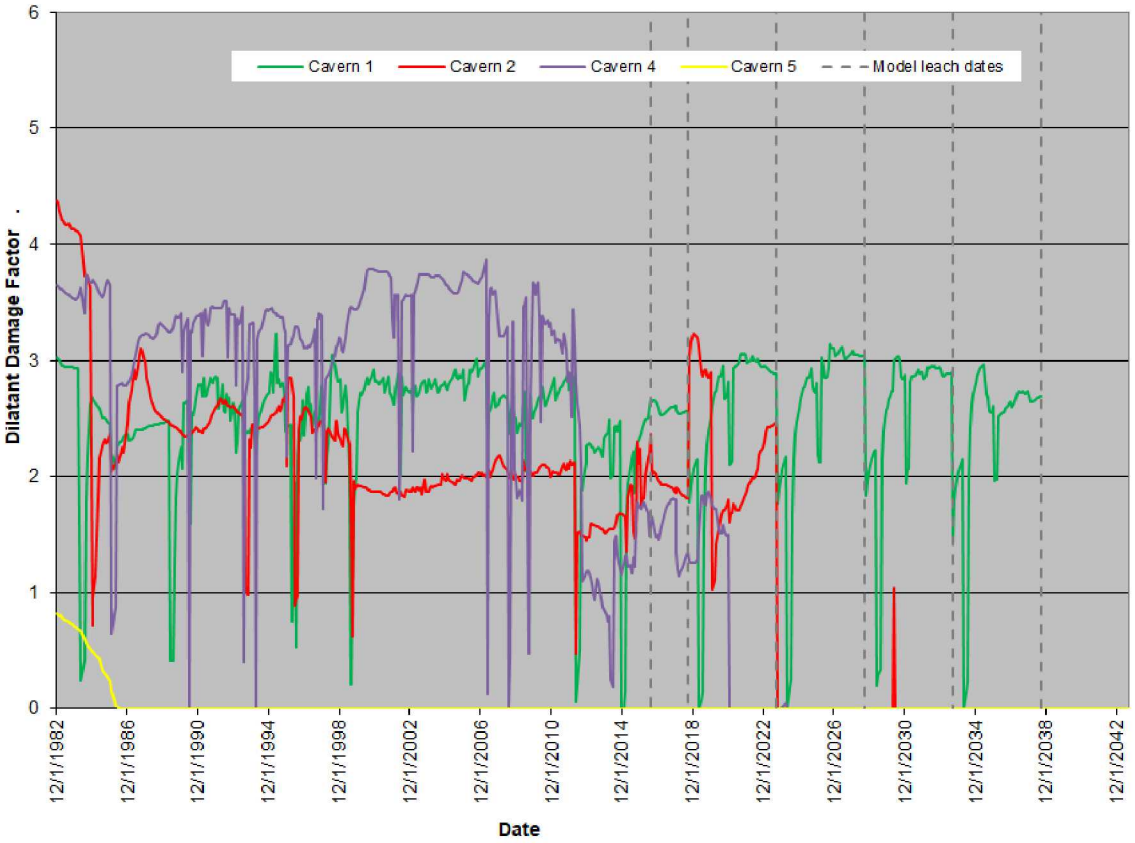

Figure 33. Predicted minimum damage factors for caverns near Caverns 1-5.

The other indicator of salt damage is the normal stress. Salt fractures under very low tensile stress (on the order of 1 MPa or 145 psi), so any indication of tension in the salt is of concern. Figure 34 shows the maximum normal stress in the salt surrounding Cavern 101-108 (base case) as a function of time; Figures 35 and 26 show the same for Caverns 109-116 and 1-5, respectively. The maximum normal stress is determined from the maximum principal stress at each location in the salt; positive values indicate tension, and negative values are compressive stresses. Much as for the damage factor, the spikes in the histories for each cavern usually represent times when that cavern is undergoing a workover. (Smaller "sub-spikes" are often one cavern's response to a neighboring cavern undergoing a workover.) For the majority of the caverns, the maximum normal stress is comfortably in the compressive regime except during workovers, when typically, an area in the cavern may experience momentary tensile stresses. These figures indicate that Caverns 105, 108, 2, 4, and 5 experience significant periods of time during their histories when some portion of the cavern exhibits tensile stress behavior. Caverns 103 and 109 show similar behavior after four or five full-cavern leaches.

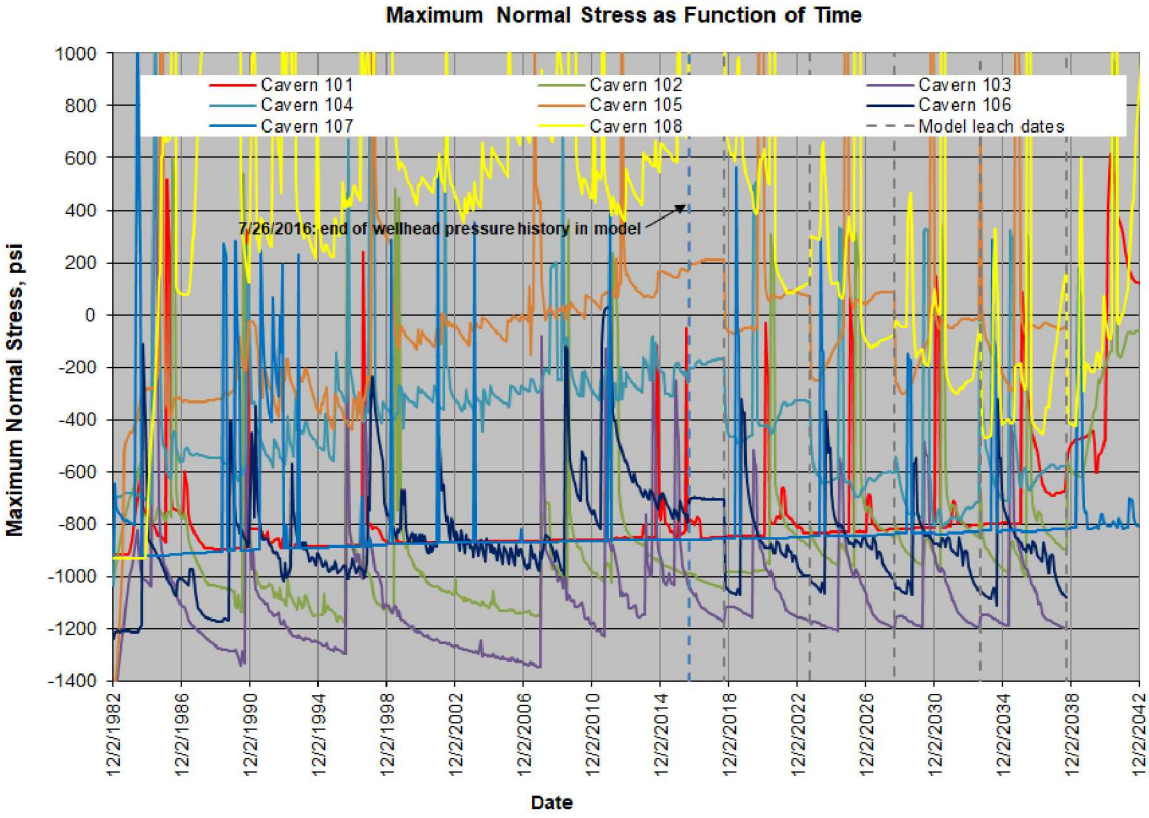

Figure 34. Maximum normal stresses in salt surrounding caverns near Caverns 101-108.

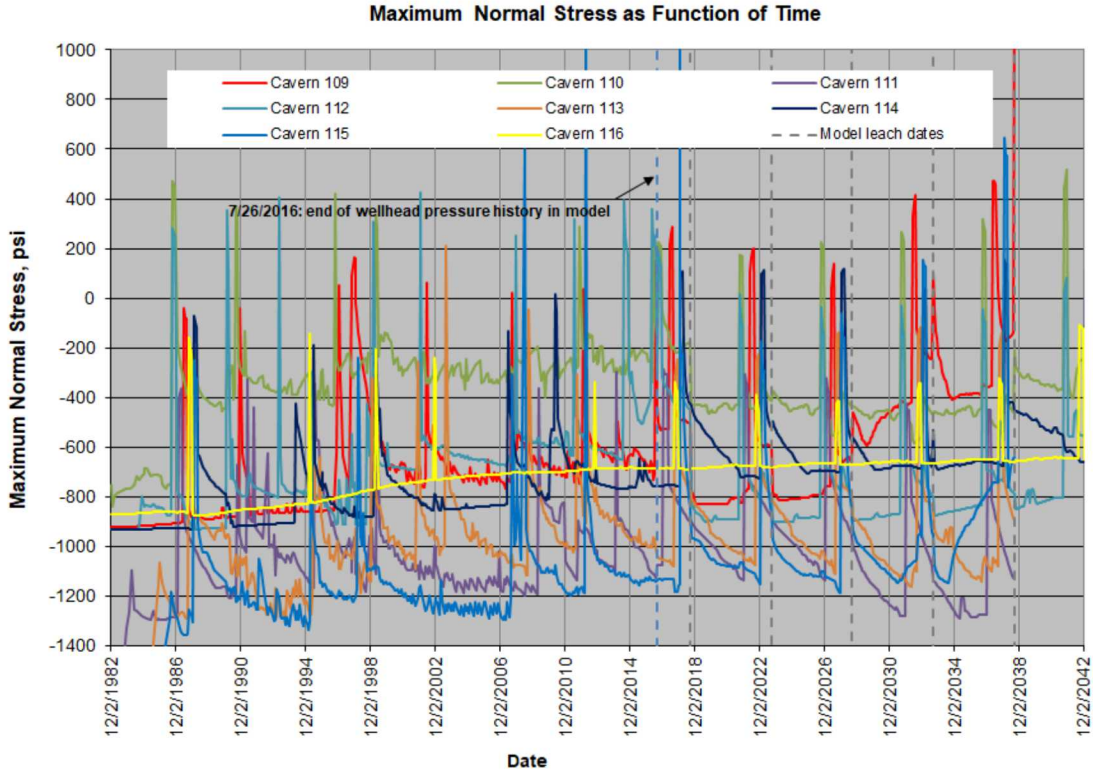

Figure 35. Maximum normal stresses in salt surrounding caverns near Caverns 109-116.

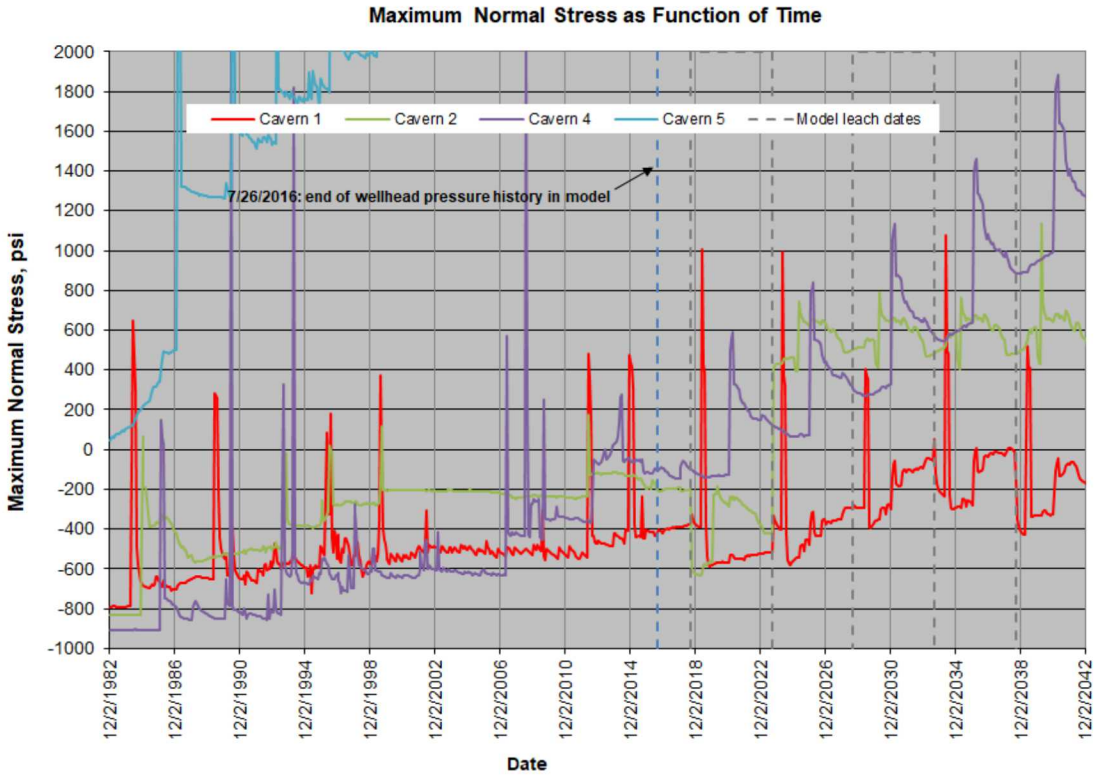

Figure 36. Maximum normal stresses in salt surrounding caverns near Caverns 1-5.

4.5 AVAILABLE DRAWDOWNS

The preceding discussion plays an important role in the assessment of the number of available drawdowns for each cavern. A drawdown of a cavern operation for which 90-100% of the oil from a cavern is removed for the purpose of sale or release to the oil market. Fresh water, or sometimes brine, is used as the replacement fluid for the cavern. The Department of Energy, in response to requests from the U.S. Congress, wishes to maintain an up-to-date table documenting the number of available full drawdowns of each of the caverns owned by the Strategic Petroleum Reserve. This information is important for assessing the SPR's ability to deliver oil to domestic oil companies expeditiously if national or world events dictate a rapid sale and deployment of the oil reserves. The evaluation of drawdown risks requires the consideration of several factors regarding cavern and wellbore integrity and stability, including stress states caused by cavern geometry and operations, salt damage caused by dilatant and tensile stresses, the effect on enhanced creep on wellbore integrity, and the sympathetic stress effect of operations on neighboring caverns.

Based on the work over the past several months, a strategy has been built for assessing the assessment of drawdown capabilities and risks for the SPR caverns (Sobolik, 2014; Sobolik et al., 2018). This strategy draws upon the results obtained from geomechanical analyses such as this one for Bryan Mound to reevaluate and update the available drawdowns for each of those caverns. Table 6 lists the updated values for the estimated available drawdowns for the Bryan Mound caverns; for historical purposes, the 2014 values are included for comparison. These estimates are based on the 2D and 3D P/D ratios for each of the Bryan Mound caverns that are

described in detail in Rudeen and Lord (2013), and the updated geomechanical computational analysis results presented in this report. Several Bryan Mound caverns are currently predicted to exhibit a 2D P/D < 1.0 on the first raw water drawdown. However, the geomechanical model evaluated the stress in the pillars between the caverns, and found that the majority of caverns should have as many as five available drawdowns. Regardless of mechanical stress conditions around the cavern, all caverns have at minimum one remaining drawdown in order to remove the oil. The results in Table 6, and the rationale and documentation of the analysis of the Bryan Mound model results to develop these new estimates for their available drawdowns, have been summarized in a letter to the DOE (Sobolik, 2018) and will be detailed in a SAND report currently in preparation.

For several of the Bryan Mound caverns, the new geomechanical calculations clearly indicate that they have at least five available drawdowns: BM-101, 102, 106, 107, 110, 111, 112, 113, 114, 115, 116. The estimates for some of the Bryan Mound caverns have dropped in value since the 2014 report because the results of the new geomechanical calculations. These drops are entirely due to the inclusion of the true cavern geometries in the finite element model. Many of the caverns have geometrical abnormalities which result in tensile stress concentrations at the locations of the abnormalities. Some of these conditions are extreme and are not likely to be easily changed, such as the large protrusion into the cavern in the bottom half of BM-105. Some caverns, like BM-104 which has a narrowed diameter around the mid-height of the cavern, may have the potential for drawdown recovery with a designed, preferential leaching from partial drawdowns. These stress conditions indicate regions around the caverns where salt cracking is likely to occur, with the most likely consequence being salt falls into the cavern. With only two exceptions, these stress concerns do not represent conditions that would cause communication with other caverns (such as West Hackberry Cavern 6) or potential cavern collapse (such as Bayou Choctaw Cavern 20); therefore, these caverns have been given estimates corresponding to the lower value derived from the geomechanical analyses and the 3D P/D values. The two exceptions are BM-2 and BM-4; because of the large diameters of the roofs of these caverns, the geomechanical analyses clearly indicate one or two available drawdowns. In the case of BM-4, several partial drawdowns at the lower depths of the cavern would be preferable than a full drawdown to the top of the cavern. BM-5 has distinct stress concentrations around the neck between the two lobes which limit the entire cavern to one available complete drawdown. However, if the lower lobe were to be permanently changed from oil to brine storage, the number of available drawdowns would likely increase.

Table 6. Updated Number of Available Drawdowns at Bryan Mound

Cavern	Basis			
	2D P/D < 1	3D P/D < 1	Geomechanics (2014)	Updated Estimate (2018)
BM101	1	4	5	5
BM102	4	5	5	5
BM103	0	3	5	2
BM104	2	3	5	3
BM105	1	4	5	2
BM106	0	2	5	5
BM107	0	4	5	5
BM108	3	4	5	2
BM109	0	2	5	3
BM110	0	2	5	5
BM111	1	3	5	5
BM112	0	2	5	5
BM113	2	4	5	5
BM114	2	5	5	5
BM115	3	4	5	5
BM116	4	4	5	5
BM1	0	0	1	2
BM2	0	0	1	1
BM4	0	0	1	2
BM5	0	0	0	1

5. CONCLUSIONS AND RECOMMENDATIONS

The results of the computational analyses lead to the following conclusions regarding the model itself, and the conditions of the caverns at Bryan Mound:

- The addition of realistic cavern geometries to the computational mesh has contributed to identification of specific cavern regions, such as in Caverns 103 and 105, which will experience long-term dilatant and tensile stress conditions due to their geometries.
- As a result, the baseline number of available drawdowns for several caverns has been reduced from five to a lower number, based on the evolution of dilatant and tensile stresses around certain caverns through planned workover and drawdown activities (Sobolik et al., 2018).
- Surface subsidence measurements continue to indicate that some phenomenon is occurring to cause enhanced subsidence over Cavern 3. A hypothesis based on previous analyses assumes that the reason for this is that brine is being forced upward from the cavern into the caprock due to creep-induced pressurization in the cavern. This behavior would correspond to a brine head in the borehole extending only up to the caprock/salt interface or slightly higher. In these calculations, a brine head for Cavern 3 was simulated to extend to above the caprock; the resulting predictions did not show a subsidence maximum over Cavern 3. These results lend credence to the hypothesis that the brine from Cavern 3 is able to enter the caprock just above the salt interface.
- The set of salt creep model properties for the new model results in predicted cavern volume reduction behavior that matches CAVEMAN-derived closure data much better than the previous Bryan Mound models. However, the resulting predictions for surface subsidence are significantly larger than the periodic subsidence data indicate.

The new model represents a more realistic assessment of the behavior of the Bryan Mound site. However, a significant amount of uncertainty still exists regarding several aspects of the model, and how they pertain to operational issues at the site. The types of uncertainty include the following items which will be addressed in future work:

- The algorithm used in CAVEMAN to calculate the daily changes to cavern volumes based on wellhead pressures, fluid temperatures, the depth of the oil/brine interface, and the geometry of the cavern, is scientifically sound. However, the parameters used in that algorithm have never been satisfactorily validated in comparison with known quantities of fluid movements into and out of the cavern. Before a new effort to develop a site-wide, cavern-specific set of salt creep parameters begins, it will be necessary to complete a study of CAVEMAN in comparison with site data to validate the algorithm and its parameters. Once there is a new historical timeline of cavern volume closure in which more confidence can be given, then a new property set in the geomechanical model may be developed, which will hopefully provide better agreement with both cavern closure and surface subsidence.
- The new model takes significantly more CPU time to run than the 2009-2012 model. This is due to a combination of factors – approximately 50% more elements in the mesh, the high aspect ratio of many elements due to the unusual cavern geometry to which they were mapped, the use of historical pressure fluctuations rather than relatively constant cavern pressures, and the use of the M-D creep model to capture transient effects. The last item regarding the M-D model may be improved soon, as members of the Sandia

computational sciences department have developed a new algorithm for calculating the strain rates in the M-D model that have reduced computation time by 90%, while producing essentially the same results. The calculations in this paper will be re-run with the new version of the model; if the results are the same and the computing performance is improved to the promised scale, then the model will have much greater utility for use in property parameterization.

- A model with improved runtime will be useful for evaluating different concepts of the effects of damage to the caprock. The model includes section of caprock that are identified as having been damaged due to sulfur mining. Previous analyses (Sobolik, 2010; Sobolik & Ehgartner, 2012b) indicated that stresses in undamaged sections of caprock may be higher than in damaged sections, as the undamaged areas much take up more of the overburden load. This could result in mechanical damage to borehole casings in those areas. Several Bryan Mound wellbores have experienced damage in the caprock, and this model should be exercised to determine if it can predict damage in those and other locations.
- A model with improved runtime performance will also be useful for scenario analysis of Cavern 3 behavior.
- A longer-term goal for this model will be to use it for testing out multiple scenarios for specific cavern operations. This can involve using the existing mesh and using different workover scenarios to test hypotheses of observed sympathetic behavior in one cavern when a nearby cavern undergoes a workover. It can also involve creating differently-shaped "onion skin" layers based on sonars or SANSMIC simulations, that illustrate the leaching effects of partial drawdowns, which are much more the normal operating mode than a full bottom-to-top drawdown. Such partial drawdown scenarios will be important for providing guidance to the DOE for tracking the available drawdown capacity for each cavern (Sobolik et al., 2018).

6. REFERENCES

- Ballard, S. and B. L. Ehgartner, 2000. *CaveMan Version 3.0: A Software System for SPR Cavern Pressure Analysis*, SAND2000-1751, Sandia National Laboratories, Albuquerque, New Mexico.
- Bauer, S. J. 1999. *Analysis of Subsidence Data for the Bryan Mound Site, Texas,* SAND99-1739, Sandia National Laboratories, Albuquerque, New Mexico.
- Blacker, T.D., S.J. Owen, M.L. Staten, W.R. Quadros, B. Hanks, B.W. Clark, R.J. Meyers, C. Ernst, K. Merkley, R. Morris, C. McBride, C. Stimpson, M. Plooster, & S. Showman, 2016. *CUBIT Geometry and Mesh Generation Toolkit 15.2 User Documentation,* SAND2016-6850R, Sandia National Laboratories, Albuquerque, New Mexico.
- Blanford, M.L., M.W. Heinstein, and S.W. Key, 2001. *JAS3D. A Multi-Strategy Iterative Code for Solid Mechanics Analysis. User's Instructions, Release 2.0*. SEACAS Library, JAS3D Manuals, Computational Solid Mechanics / Structural Dynamics, Sandia National Laboratories, Albuquerque, New Mexico.
- Ehgartner, B.L., 2004. "Incorporation of Compressibility Model and other enhancements/ upgrades into Caveman," Letter to R.E. Myers, DOE-SPR, March 31, 2004, Sandia National Laboratories, Albuquerque, New Mexico.
- Ehgartner, B.L., 2009. "Subtask 1.3 Activity A4 Re-Optimization of Caveman Parameters," Letter to R.E. Myers, DOE-SPR, April 29, 2009, Sandia National Laboratories, Albuquerque, New Mexico.
- Hogan, R. G., ed., 1980. *Strategic Petroleum Reserve (SPR) Geological Site Characterization Report: Bryan Mound Salt Dome*, SAND80-7111. Sandia National Laboratories, Albuquerque, NM.
- Keplinger and Associates, 1980. "Report of Investigations on Cavern #3, Bryan Mound Strategic Petroleum Reserve, Freeport, Texas," for Dravo Utility Constructors Inc. and U.S. Department of Energy, New Orleans, Louisiana, August 30, 1980.
- Kirby, C.L. and A.S. Lord, 2015. *Sulphur Extraction at Bryan Mound,* SAND2015-6827, Sandia National Laboratories, Albuquerque, New Mexico.
- Lama, R.D. and V.S. Vutukuri, 1978. *Handbook on Mechanical Properties of Rocks – Testing Techniques and Results*, Series on Rock and Soil Mechanics, Vol. 3, No.2, Trans Tech Publications.
- Lord, A.S., 2007a. "January 2007 Bryan Mound Subsidence Analysis," Letter Report to R. Myers, DOEPMO, April 11, 2007.
- Lord, A.S., 2007b. "An Updated Three-Dimensional Site Characterization Model of the Bryan Mound Strategic Petroleum Reserve Site, Texas," Letter Report to W. Elias, DOE PMO, November 5, 2007.
- Lord, A.S., 2009. "April 2009 Bryan Mound Subsidence Analysis," Letter Report to R. Myers, November 16, 2009.
- Lord, A.S., 2010. "October 2010 Bryan Mound Subsidence Analysis," Letter Report to W. Elias, March 24, 2010.
- Morgan, H.S. and R.D. Krieg, 1990. *Investigation of an Empirical Creep Law for Rock Salt that Uses Reduced Elastic Moduli*, SAND89-2322C, presented at the 31st U.S. Symposium

on Rock Mechanics held in the Colorado School of Mines in June 18-20, 1990, Sandia National Laboratories, Albuquerque, New Mexico.

- Munson, D.E., 1998. *Analysis of Multistage and Other Creep Data for Domal Salts*, SAND98-2276, Sandia National Laboratories, Albuquerque, New Mexico.
- Neal, J.T., T.R. Magorian, and S. Ahmad, 1994. *Strategic Petroleum Reserve (SPR) Additional Geologic Site Characterization Studies Bryan Mound Salt Dome, Texas*, SAND94-2331. Sandia National Laboratories, Albuquerque, New Mexico.
- Osnes, J.D., 1995. "Update to Subsidence Analyses of Strategic Petroleum Reserve Sites for Fiscal Years 1993 and 1994," Topical Report RSI-0590, RE/SPEC, Rapid City, South Dakota.
- Park, B.Y. and B.L. Ehgartner, 2009. *Sensitivity of Storage Field Performance to Geologic and Cavern Design Parameters in Salt Domes,* SAND2009-1278, Sandia National Laboratories, Albuquerque, New Mexico.
- Park, B. Y., B.L. Roberts, and S.R. Sobolik. 2017. Construction of hexahedral finite element mesh capturing realistic geometries of a petroleum reserve. *Journal of Finite Elements in Analysis and Design*, 135, 68–78. https://doi.org/10.1016/j.finel.2017.07.007.
- Park, B. Y., S.R. Sobolik, and C.G. Herrick. 2018. Geomechanical Model Calibration Using Field Measurements for a Petroleum Reserve. *Journal of Rock Mechanics and Rock Engineering*, ISSN 0723-2632, https://doi.org/10.1007/s00603-017-1370-4.
- Preece, D.S. and J.T. Foley, 1984. *Long-Term Performance Predictions for Strategic Petroleum Reserve (SPR) Caverns*, SAND83-2343, Sandia National Laboratories, Albuquerque, New Mexico.
- Rautman, C.A. and A. Snider Lord, 2007. *Sonar Atlas of Caverns Comprising the U.S. Strategic Petroleum Reserve Volume 3: Bryan Mound Site, Texas*, SAND2007-6067, Sandia National Laboratories, Albuquerque, New Mexico.
- Sobolik, S.R. and B.L. Ehgartner, 2009. *Analysis of Cavern Stability at the Bryan Mound SPR Site,* SAND2009-1986, Sandia National Laboratories, Albuquerque, New Mexico.
- Sobolik, S.R. and B.L. Ehgartner, 2009a. *Analysis of Cavern Stability at the West Hackberry SPR Site,* SAND2009-2194, Sandia National Laboratories, Albuquerque, New Mexico.
- Sobolik, S.R., 2010. "Geomechanical Analysis of the Bryan Mound SPR Site with Mining-Induced Damage in the Caprock," Letter Report to R. Myers, July 13, 2010.
- Sobolik, S.R. and B.L. Ehgartner, 2012a. *Analysis of the Stability of Cavern 3 at the Bryan Mound SPR Site,* SAND2012-1953, Sandia National Laboratories, Albuquerque, New Mexico.
- Sobolik, S.R. and Ehgartner, B.L., 2012b. Structural Integrity of Oil Storage Caverns at a Strategic Petroleum Reserve Site with Highly Heterogeneous Salt and Caprock. In *Proceedings of the 46th U.S. Rock Mechanics Symposium,* ARMA 12-189*,* Chicago, Illinois, June 24-27, 2012.
- Sobolik, S., 2014. "Current Recommendations Regarding ECP PM-00449, Baseline Remaining Drawdowns for all SPR Caverns." Letter to Lisa Nicholson, May 8, 2014, DOE-SPR, Sandia National Laboratories. U.S. Strategic Petroleum Reserve.
- Sobolik, S.R. and Lord, A.S., 2014. Case Study of the Impact of Prior Cavern Abandonment on Long-Term Oil Storage at a Strategic Petroleum Reserve Site. In *Proceedings of the 48th U.S. Rock Mechanics Symposium,* ARMA 14-7002*,* Minneapolis, Minnesota, June 1-4, 2014.

- Sobolik, S. R., D. Hart, B.Y. Park and K. Chojnicki, 2018. " Proposed Methodology for Assessing Available Drawdowns for Each Oil Storage Cavern in the Strategic Petroleum Reserve." SAND2018-4518, Sandia National Laboratories, Albuquerque, NM USA. U.S. Strategic Petroleum Reserve.
- Stein, J.S. and Rautman, C.A., 2005. *Conversion of the Bryan Mound Geological Site Characterization Reports to a Three-Dimensional Model*, SAND2005-2009, Sandia National Laboratories, Albuquerque, New Mexico.
- Thorton, C.H and I.P. Lew, 1983. *Concrete and Design Construction. Standard Handbook for Civil Engineers*, Chapter 8, 3rd ed., F.S. Merritt, editor, McGraw-Hill, New York, NY.
- Van Sambeek, L.L., J.L. Ratigan, and F.D. Hansen, 1993. *Dilatancy of Rock Salt in Laboratory Tests*, Int. J. Rock Mech. Min. Sci. & Geomech. Abstr. Vol. 30, No. 7, pp 735-738.
- Wawersik, W.R. and D.H. Zeuch, 1984. *Creep and Creep Modeling of Three Domal Salts – A Comprehensive Update*, SAND84-0568, Sandia National Laboratories, Albuquerque, New Mexico.

DISTRIBUTION:

External Distribution

Electronic copies to:

Wayne Elias (wayne.elias@hq.doe.gov)
for distribution to DOE SPR Program Office, Washington, D.C.
U.S. Department of Energy
Office of Fossil Energy
Forrestal Building
1000 Independence Ave., SW
Washington, DC 20585

Diane Willard (diane.willard@spr.doe.gov)
for distribution to DOE and FFPO SPR Project Management Office, New Orleans, LA.
U.S. Department of Energy
Strategic Petroleum Reserve Project Management Office
900 Commerce Road East
New Orleans, LA 70123

Sandia Distribution

Print copies to:

1 MS0706 Anna C. Snider Lord 8862 (print and electronic copy)
0 MS0706 D. L. Lord 8862 (electronic copy)
0 MS0735 E. K. Webb 8860 (electronic copy)
0 MS0750 G. Bettin 8812 (electronic copy)
0 MS0750 D. M. Moriarty 8862 (electronic copy)
0 MS0750 K. Chojnicki 8862 (electronic copy)
5 MS0750 C. L. Kirby 8863 (print and electronic copies)
0 MS0751 B. L. Roberts 8862 (electronic copy)
1 MS0751 B. Y. Park 8862 (print and electronic copies)
1 MS0751 S. R. Sobolik 8862 (print and electronic copy)
0 MS0751 D. Hart 8862 (electronic copy)

0 MS0899 Technical Library 9536 (electronic copy)

Sandia National Laboratories